Mast cells promote pathology and susceptibility in tuberculosis

Ananya Gupta[1,2#], Vibha Taneja[1#], Javier Rangel Moreno[3], Nilofer Naqvi[1], Abhimanyu[1], Yun Tao[1], Mushtaq Ahmed[1], Kuldeep S. Chauhan[1], Daniela Trejo-Ponce de León[5,6], Gustavo Ramírez-Martínez[6], Luis Jiménez-Alvarez[6], Cesar Luna-Rivero[6], Joaquin Zuniga[5,6], Deepak Kaushal[6], Shabaana A. Khader[1,2#]

Affiliations:

[1]The University of Chicago, Department of Microbiology, 920 East 58th Street, CLSC 1117, Chicago, IL 60637.

[2] Department of Molecular Microbiology, Washington University in St. Louis, St. Louis, MO 63110, USA

[3] Division of Allergy, Immunology and Rheumatology, Department of Medicine, University of Rochester Medical Center, Rochester, NY, USA

[5] Technologico de Monterrey, Escuela de Medicina y Ciencias de la Salud, Mexico City, Mexico

[6] Laboratory of Immunobiology and Genetics and Department of Pathology, Instituto Nacional de Enfermedades Respiratorias Ismael Cosio Villegas, Mexico

[7] Texas Biomedical Research Institute, San Antonio, Texas 78245-0549, USA.

[#] Equal first authorship

Correspondence: Shabaana A. Khader, The University of Chicago, Department of Microbiology, 920 East 58th Street, CLSC 1117, Chicago, IL 60637, Phone: (773)-702-2601. Email-khader@uchicago.edu

Abstract

Tuberculosis (TB), caused by the bacterium *Mycobacterium tuberculosis* (*Mtb*), infects approximately one-fourth of the world's population. We reported an increased accumulation of mast cells (MCs) in the lungs of macaques with active pulmonary TB (PTB), compared with those with latent TB infection (LTBI). MCs respond in vitro to *Mtb* exposure via degranulation and by inducing proinflammatory cytokines. In the current study, we demonstrate an increased production of chymase by MCs in granulomas of humans and macaques with PTB. Single-cell (sc) RNA sequencing analysis revealed distinct MC transcriptional programs between LTBI and PTB, with PTB associated MCs enriched in interferon gamma, oxidative phosphorylation, and MYC signaling. In a mouse model, MC deficiency led to improved control of *Mtb* infection that coincided with reduced accumulation of lung myeloid cells and diminished lung inflammation at chronic stages of infection. Airway transfer of MCs into wild-type *Mtb*-infected mice showed increased neutrophils, decreased recruited macrophages, and elevated *Mtb* dissemination to the spleen. Together, these findings highlight MCs as active drivers of TB pathogenesis and potential targets for host-directed therapies for TB.

Keywords: Mast cells, Tuberculosis, lung, innate cell, inflammation.

40 **Introduction**

41 Tuberculosis (TB) remains a significant global health issue, with approximately one-quarter of
42 the world's population harboring *Mycobacterium tuberculosis* (*Mtb*), causing around 1.25
43 million deaths each year (WHO, 2024). The disease often starts as a latent TB infection (LTBI),
44 in which the bacteria may remain dormant without disease symptoms. However, LTBI can
45 progress to active pulmonary TB (PTB), characterized by severe respiratory symptoms and
46 high transmission potential. The immune mechanisms that allow progression from latency to
47 PTB are not fully defined. Thus, understanding the immune factors that drive progression
48 toward PTB will allow the development of novel therapeutics for TB control. Towards this
49 overall goal, we recently showed that the lung single-cell transcriptional immune landscape
50 during LTBI and PTB in *Mtb*-infected macaques was distinct. For example, PTB was
51 characterized by the significant accumulation of Type I IFN-expressing plasmacytoid DCs
52 (pDCs), IFN-responsive macrophages, as well as activated T cells in the lungs (Esaulova et al.,
53 2021). Additionally, mast cells (MCs) were increased in the lungs of macaques with PTB
54 (Esaulova et al., 2021). In sharp contrast, LTBI was characterized by increased presence of
55 cytotoxic NK cells but lack of recruitment of MCs in the lungs (Esaulova et al., 2021).

56 MCs are found in the lung where they influence inflammatory responses (Virk et al., 2016;
57 Wasserman, 1984). MCs have been shown to respond *in vitro* to *Mtb* exposure via surface
58 receptors such as CD48 (Munoz et al., 2003). They also respond to *Mtb* exposure or
59 mycobacterial lipids by undergoing degranulation of prestored granules, such as histamine and
60 β-hexosaminidase, and secrete proinflammatory cytokines such as IL-6 and TNF-α (Munoz et
61 al., 2003). Degranulation of MCs following intratracheal infection with a high dose of *Mtb* was
62 shown to limit inflammation and the production of proinflammatory cytokines such as IL-1β
63 and TNF-α (Carlos et al., 2007). MCs produce and release either chymase or tryptase (Bian et
64 al., 2021), which are both proteases that are stored in the cell's secretory granules. Recent

65 studies with lung biopsies of TB patients showed an enrichment of MCs expressing IL-17 at
66 inflammatory sites. In contrast, chymase-rich MCs (MC_Cs) producing TGF-β were detected in
67 proximity to mature granulomas in lung biopsies from PTB (Garcia-Rodriguez et al., 2021).
68 Furthermore, while healthy lung predominantly has tryptase-expressing mast cells (MC_Ts),
69 both chymase and mast cells co-expressing chymase and tryptase (MC_Cs and MC_{TC}s)
70 accumulate in the infected lung of patients with PTB (Garcia-Rodriguez et al., 2021). Thus,
71 while previous studies have shown that MCs respond to *Mtb* exposure and accumulate in
72 macaque and human lungs during PTB, it is not completely known if MCs functionally mediate
73 protective or pathological outcomes in the context of TB infection.
74 In the current study, we showed that the distribution and localization of MCs in PTB in humans
75 and macaques were associated with chymase production. Using scRNA seq analysis, we show
76 that MCs found in LTBI and healthy lungs in macaques are transcriptionally distinct from PTB
77 lungs, showing enrichment of tumor necrosis factor alpha, cholesterol, and transforming
78 growth factor beta signaling. In contrast, MCs found in PTB express increased levels of
79 signatures associated with interferon gamma, oxidative phosphorylation, and MYC signaling.
80 Additionally, mice deficient in MCs showed improved control of *Mtb* infection and reduced
81 lung inflammation. Airway transfer of MCs into wild-type *Mtb*-infected mice increased lung
82 neutrophils and elevated *Mtb* dissemination to the spleen. These results together provide novel
83 evidence that MCs contribute to immune pathology and reduced *Mtb* control, suggesting a
84 pathological role for MCs during *Mtb* infection.

85 **Materials and methods**

86 **Study subjects and animal studies**

87 All human lung biopsy samples were obtained from the Tuberculosis Outpatient Clinic and the
88 Department of Pathology at the National Institute of Respiratory Diseases (INER) in Mexico
89 City, before *Mtb* treatment with informed consent, and with the approved protocol by the INER

90 IRB for their use (project numbers B04-15 and B09-23). Also, lung samples from healthy
91 controls (HC), non-TB individuals, were obtained from the tissue repository of the Department
92 of Pathology at INER. No compensation was provided to the patients.
93 Non-human primate procedures were approved by the Institutional Animal Care and Use
94 Committee of Tulane National Primate Research Center and were performed following
95 National Institutes of Health (NIH) guidelines. Male and female Indian rhesus macaques,
96 verified to be free of *Mtb* infection by tuberculin skin test, were obtained from the Tulane
97 National Primate Research Center. The animals were housed in an ABSL3 facility.
98 C57BL/6 and B6.Cg-KitW-sh/HNihrJaeBsmJ (Strain #:030764) alias $CgKitW^{sh}$ mice were
99 procured from Jackson Laboratory (Bar Harbor, ME) and bred at Washington University in St.
100 Louis or University of Chicago. Six to eight-week-old female and male mice were used in the
101 experiments. All mice were maintained and used per the approved Institutional Animal Care
102 and Use Committee (IACUC) guidelines at Washington University in St. Louis or University
103 of Chicago.
104
105 **Aerosol infection**
106 For murine experiments, *Mtb* strain HN878 was cultured in Proskauer Beck medium containing
107 0.05% Tween 80 until reaching mid-log phase and frozen in 1 ml aliquots at -80°C until used.
108 Mice were aerosol infected with ~100 colony-forming units (CFU), as described previously
109 (Khader et al., 2007). *Mtb* strain CDC1551 was used to infect NHPs. This species-specific
110 choice reflects differences in pathogenicity: HN878 induces robust disease in mice, while
111 CDC1551, a less virulent strain, allows development of a macaque model that recapitulates
112 latent and chronic TB upon low- to moderate-dose aerosol exposure respectively (Kaushal et
113 al., 2015; Sharan et al., 2021; Singh et al., 2025). This ensures physiologically relevant and
114 controlled studies within each species. Macaques were assigned to three groups: (1) uninfected

115 control, (2) macaques with LTBI were exposed to a low dose (~10 CFU), and (3) macaques
116 with PTB were exposed to a high dose (~100 CFU) of *Mtb* CDC1551 via the aerosol route
117 using a custom head-only dynamic inhalation system housed within a class III biological safety
118 cabinet as previously described (Esaulova et al., 2021). The animals were periodically
119 monitored for their physiological parameters and to monitor disease symptoms.

120 **Bacterial burden and cytokine analysis**

121 Bacterial burden was assessed using serial 10-fold dilutions of lung or spleen homogenates and
122 plated on 7H11 agar solid medium supplemented with OADC (oleic acid, bovine albumin,
123 dextrose, and catalase). Colonies were counted after 2-3 weeks of incubation.
124 Cytokine/chemokine expression was analyzed in lung homogenates from infected mice via
125 Luminex (Millipore-Sigma) or ELISA (R&D) as per the manufacturer's protocol.

126 **Generation of single-cell suspensions from tissues and flow cytometry staining**

127 Lung single-cell suspensions from *Mtb*-infected mice were prepared as previously described,
128 (Gopal et al., 2013). Briefly, mice were euthanized with CO_2. The right lower lobe was isolated
129 and perfused with heparin in saline. Lungs were minced and incubated with collagenase/DNase
130 for 30 minutes at 37°C. Lung tissue was pushed through a 70µm nylon screen to obtain a single-
131 cell suspension. Following lysis of erythrocytes, the cells were washed and resuspended in
132 cDMEM (DMEM high glucose + 10% fetal bovine serum + 1% Penicillin/Streptomycin) for
133 flow cytometry staining. For flow cytometric analysis, cells were either stained immediately
134 or stimulated with phorbol myristate acetate (PMA-50ng/ml; Sigma Aldrich) and ionomycin
135 (750 ng/ml; Sigma Aldrich) in the presence of GolgiStop (BD Pharmingen).

136 For myeloid cell surface staining, the following fluorochrome-conjugated antibodies were
137 used: CD11b-APC (clone M1/70), CD11c-PE-Cy7 (clone HL3, BD Biosciences), GR-1-
138 PerCP-Cy5.5 (clone RB6-8C5, BD Pharmingen), and MHC class II-FITC (clone M5/114.15.2,
139 Tonbo Biosciences), CD117 (cKit)-Super Bright 780 (clone 2BB, eBioscience), and FcεR1-

140 PE (clone MAR-1, eBioscience). Myeloid cell subsets were defined as follows: alveolar
141 macrophages ($CD11c^{+}CD11b^{-}$), neutrophils ($CD11b^{+}CD11c^{-}Gr\text{-}1^{hi}$), monocytes
142 ($CD11b^{+}CD11c^{-}Gr\text{-}1^{med}$), recruited macrophages ($CD11b^{+}CD11c^{-}Gr\text{-}1^{low}$), and MCs
143 ($CD11b^{-}cKit^{+}Fc\varepsilon R1^{+}$). T cells were identified based on a gating strategy as described before
144 (Griffiths et al., 2016)). Surface staining included CD3-AF700 (clone 500A2, BD Biosciences),
145 CD4-Pacific Blue (clone RM4.5, BD Biosciences), CD44-PE-Cy7 (clone 1M7, Tonbo
146 Biosciences), and CD8-APC-Cy7 (clone 53-6.7, BD Biosciences). For intracellular cytokine
147 staining, lung cells were fixed and permeabilized using fixation/permeabilization concentrate
148 and diluent (eBioscience) following the manufacturer's instructions. Cells were then stained
149 with IFNγ-APC (clone XMG1.2, Tonbo Biosciences) and TNF-α-FITC (clone MP6-XT22, BD
150 Pharmingen), or respective isotype controls (APC rat IgG1κ and FITC rat IgG1α, BD
151 Pharmingen) for 30 minutes. Samples were acquired on a four-laser BD Fortessa Flow
152 Cytometer, and data were analyzed using FlowJo software (Treestar). Absolute cell numbers
153 for each population were back calculated based on total viable cell counts per lung sample.

154 **In vitro culture and intratracheal delivery of MCs**

155 Six to eight weeks old C57BL/6 mice were euthanized by CO_2, and femurs and tibia were
156 collected. Bone marrow cells obtained after RBC lysis were suspended in Bone Marrow
157 Derived MC (BMMC) media containing RBMI media (Gibco) supplemented with 20% FBS
158 (Sigma), 4mM- glutamine (Sigma), 25mM HEPES (Corning), 5 x 10^{-5} 2- mercaptoethanol
159 (Sigma), 1mM sodium pyruvate (Sigma), 0.1mM nonessential amino acids (Gibco), Penicillin
160 and Streptomycin (Sigma), 20ng/ml murine IL-3 and 20ng/ml murine Stem Cell factor
161 (Peprotech) and maintained in BMMC media at 1 X 10^{6} cells per ml in T75 flasks at 37°C in
162 5% CO2 incubator. Cells were fed twice every week with fresh BMMC media by centrifuging
163 non-adherent cells at 1000 rpm for 10 min at room temperature, resuspending at a density of
164 1x10^{6}/ml, and were maintained for 30 days. At 30 days, more than 95% cells were positive for

165 FcεRI and c-kit, which was confirmed by flow cytometry (Varma & Puri, 2019) . $5x10^4$ BMMC
166 having 95% FcεRI and c-kit positivity were transferred in C57Bl/6 through the intratracheal
167 route.

168 **Morphometric analysis of lung Histopathology and neutrophil infiltration**

169 For mouse studies, the left upper lobe was collected for histomorphometric analysis. The lobes
170 were infused with 10% neutral buffered formalin and embedded in paraffin. 5 μm-thick lung
171 sections were cut using a microtome, stained with hematoxylin and eosin (H&E), and
172 processed for light microscopy. Images were captured using the automated Nanozoomer digital
173 whole slide imaging system (Hamamatsu Photonics). Regions of inflammatory cell infiltration
174 were delineated utilizing the NDP view2 software (Hamamatsu Photonics), and the percentage
175 of inflammation was calculated by dividing the inflammatory area by the total area of
176 individual lung lobes. All scoring was conducted in a blinded manner. Formalin-Fixed Paraffin
177 Embedded (FFPE) lung sections were also stained with APC-conjugated rat anti-mouse Ly6G
178 (clone 1A8, BioLegend, RRID:AB_2227348). Nuclei were counterstained with DAPI.
179 Neutrophils were quantified in three randomly selected 200× fields per lung section. Images at
180 200× magnification were acquired using a Zeiss Axioplan microscope and recorded with a
181 Hamamatsu camera.

182 FFPE lung sections from healthy individuals, tuberculosis patients, and NHP infected with
183 *Mtb* were stained with goat anti-human mast cell chymase (LifeSpan Biosciences, LS-B4134,
184 RRID: AB_10718418) and rabbit anti-human tryptase (Cell Signaling Technology, 195235).
185 Primary antibodies were detected with Alexa Fluor 568 donkey anti-goat IgG (Thermo Fisher
186 Scientific, A-11057, RRID: AB_2534104) and Alexa Fluor 488 donkey anti-rabbit IgG
187 (Jackson ImmunoResearch Laboratories, 711-546-152, RRID: AB_2340619). Nuclei were
188 labeled with DAPI. MC positive for chymase, tryptase, or both were blindly quantified in three

189 200x random fields per sample in human and NHP lung sections. 200x pictures were taken
190 with an Axioplan Zeiss microscope and recorded with a Hamamatsu camera.
191
192 **Single-cell data reanalysis**
193 The NHP single cell lung data was accessed from GEO (GSE149758) and processed through
194 Cell Ranger v7.0 using the Macaca Mulatta reference genome (Mmul_10). The obtained
195 matrix file was processed through the R package *Seurat v5* for downstream analysis of the
196 count matrix. The cells were filtered based on mitochondrial gene content and were selected
197 for analysis when at least 500 genes were detected. Data was log normalized. The most variable
198 genes were detected by the *FindVariableFeatures* function and used for subsequent analysis.
199 Latent variables (number of UMIs and mitochondrial content) were regressed out using a
200 negative binomial model (function *ScaleData*). Principal component analysis (PCA) was
201 performed with the *RunPCA* function. A UMAP dimensionality reduction was performed on
202 the scaled matrix (with most variable genes only) using the first 20 PCA components to obtain
203 a two-dimensional representation of the cell states. For clustering, we used the functions
204 *FindNeighbors* (20 PCA) and *FindClusters* (resolution 0.25). MCs were identified and re-
205 clustered based on expression of the canonical MC marker genes *FCER1A* (High affinity Fc
206 IgE receptor), *CD48*, *FCER1G* (Fc IgE receptor), *MS4A2* (IgE subunit), and *ITGAX* (CD11c)
207 as a negative marker. The cells identified MC cluster (only one cluster) were subset and re-
208 clustered using the method outlined above at a resolution of 0.1. To identify marker genes for
209 mast cells, we used *FindAllMarkers* to compare the cluster against all other clusters and
210 *FindMarkers* to compare selected clusters. For each cluster, only genes that were expressed in
211 more than 15% of cells with at least 0.15-fold differences were considered. The differential
212 genes were subjected to enrichment analysis using the Hallmark Pathway gene set from
213 *MsigDB*. Only the pathways that met an FDR threshold less than 0.05 were considered. Gene

214 signatures were defined with the R package *Ucell*. The output is a module signature score
215 generated by the *AddModuleScore* function. The obtained score was overlaid on the UMAP
216 and visualized. The Values per cell were extracted and used to plot a summed module U cell
217 score. GraphPad Prism was used for the Violin plots and the heatmap. All other figures were
218 generated in R.

219 An independent *M. fascicularis* lung single-cell RNA-seq dataset (GSE200151) (Gideon et al.,
220 2022) was downloaded and processed using Cell Ranger v7.0 with the *Macaca mulatta*
221 reference genome (Mmul_10). The resulting count matrices were imported into Seurat v5 for
222 downstream analysis. Cells were filtered based on mitochondrial gene content and were
223 retained if they expressed at least 500 genes. Data were log-normalized, the most variable genes
224 were identified with *FindVariableFeatures*, and confounding effects of sequencing depth
225 (UMI counts) and mitochondrial fraction were regressed out during scaling with ScaleData.
226 Principal component analysis (PCA) was performed, followed by clustering *(FindNeighbors,*
227 *FindClusters*) and UMAP embedding (*RunUMAP*). MCs were identified and subset based on
228 canonical marker expression (*FCER1A*, *CD48*, *FCER1G*, *MS4A2*) and re-clustered at low
229 resolution to ensure purity of the MC population. To quantify MC subsets across disease
230 severity states, we calculated the proportion of cells expressing chymase (*CMA1*), tryptase
231 (*LOC102140229*, *TPSG1*), or dual-positive $CMA1^{+}LOC102140229^{+}$ using binary thresholds
232 (>0 counts). Fisher's exact tests were performed to compare proportions between MCs from
233 high-burden granulomas (4 weeks, more severe disease; n = 372 MCs) and low-burden
234 granulomas (10 weeks, less severe disease; n = 7,306 MCs). For each comparison, we reported
235 the odds ratio (OR) with 95% confidence interval and the exact *p*-value. To examine functional
236 programs, we computed UCell signature scores for Hallmark IFNγ signaling, TNF signaling,
237 and oxidative phosphorylation. Signature score distributions were compared between severity
238 groups. All statistical tests were performed in R (v4.3.1) with the Seurat (v5.0) and UCell (v2.0)

239 packages. Violin and bar plots were generated in R or exported to GraphPad Prism for
240 visualization.

241 **Data analysis and statistics**

242 All data were analyzed using the indicated methodology in each figure legend. Two-sided
243 unpaired t-test was performed for comparing the significance between 2 groups, one-way
244 ANOVA, Tukey's test, and two-way ANOVA Sidak's multiple comparison test was performed
245 for more than 2 groups using GraphPad Prism 5 and 10, respectively (La Jolla, CA).
246 Significance is denoted on the figure and the respective figure legends. Outliers, if any, were
247 removed using Grubb's outlier test and mentioned in the respective figures.

248

249 **Results**

250 **Mast cells localize and transition phenotypes within TB granulomas**

251 A previous study observed that tryptase-expressing MC_Ts were primarily found within the
252 lungs of healthy controls (HC), while chymase-expressing MC_Cs or both chymase and tryptase-
253 expressing MC_{TC}s were found in the lung of patients with PTB (Garcia-Rodriguez et al., 2021).
254 To corroborate these observations and analyze the compartmentalization of MCs in human
255 lungs, we stained lung biopsies from healthy individuals and patients with PTB to visualize the
256 spatial distribution of MC_Ts, MC_Cs, and MC_{TC}s. Lung granulomas from PTB patients were
257 further classified by the presence or absence of necrosis, as early or late granulomas. Early
258 granulomas had well-defined immune and stromal cell clusters without central necrosis. Late
259 granulomas were larger, with necrotic cores containing bacteria and dead neutrophils,
260 surrounded by lymphocytes.
261 MCs were quantified both within and around early granulomas, whereas in late granulomas,
262 they were primarily measured in the peripheral regions surrounding the necrotic center.

263 Considering lung parenchyma, interstitium, vasculature, or bronchus, we observed that HC
264 lungs predominantly contain MC_Ts and, to a lesser extent, MC_{TC}s. In TB lesions from PTB
265 patients, MC_{TC}s accumulated in early immature granulomas, whereas MC_Cs accumulated in
266 late granulomas (Figure 1A-B). MC_Ts also increased in the interstitium, vasculature, and
267 bronchus-associated lymphoid tissue of PTB patients (Figure S1A-C). However, we did not
268 observe any differences in MC_{TC}s and MC_Cs at these sites (Figure S1D-I). These observations
269 confirmed that tryptase-expressing MC_Ts are found in HCs (Garcia-Rodriguez et al., 2021),
270 while the dual tryptase and chymase-expressing MCs were seen in early granulomas, and only
271 chymase-associated MCs were observed in late granulomas with necrotic cores, defined the
272 MCs associated with TB disease progression.
273 Our previously published data showed that MCs accumulate in the lungs of macaques with
274 PTB compared to LTBI (Esaulova et al., 2021). Thus, we next analyzed the accumulation and
275 localization of MCs in the lungs of macaques with LTBI and PTB. We found that, similar to
276 human healthy lungs, MC_Ts accumulated in the lungs of healthy macaques. Although MC_Ts
277 increased in some lesions in the lungs of macaques with LTBI, the numbers of MC_Ts in
278 macaques with PTB were significantly increased in all sites, including the granuloma (Figure
279 1C-D), interstitium, vasculature, as well as bronchus-associated lymphoid tissue of PTB
280 patients (Figure S1J-L). Additionally, MC_{TC}s were significantly increased within the
281 granulomas of macaques with PTB compared to the lungs of macaques with LTBI and HCs
282 (Figure 1C-D), but did not differ at any other sites in the lung (Figure S1M-O) compared to
283 HCs. However, we did not observe any increase in these cells at other sites within the lung
284 compared to healthy macaques. MC_Cs were not measurable in any region of the macaque lungs.
285 Our data indicate that during LTBI, there is an accumulation of MC_Ts but not MC_{TC}s. However,
286 as the disease progresses to PTB, both MC_{TC}s and additional MC_Ts are elevated, particularly
287 within the granulomatous lesions.

288 **Lung single-cell transcriptome in macaques with tuberculosis exhibits MC diversity**

289 In the previous section, we found that tryptase protein expression on MCs was lower in LTBI,
290 and as the disease progressed to PTB, MCs expressed chymase, either alone MC_Cs or in
291 combination with tryptase, MC_{TC}. To further validate whether this increase in tryptase and
292 chymase protein expression was also reflected in the single-cell transcriptomes during PTB,
293 LTBI, and HCs, we re-analyzed the MCs from our previously published data from NHPs
294 (Esaulova et al., 2021). These macaques were infected with 10 bacilli to generate LTBI, or
295 with 100 bacilli for a progressive PTB infection, or were uninfected (Figure 2A). The median
296 duration of infection for the PTB macaques was 10 weeks, and the LTBI macaques underwent
297 necropsy at a median of 23 weeks post-infection. We analyzed the single-cell transcriptomes
298 of 500 MCs using unsupervised clustering and identified four distinct clusters. Three clusters
299 (0, 1, and 3) belonged to the PTB group, while cluster 2 was found exclusively in LTBI and
300 HC, with the majority of MCs coming from the PTB condition (Figure 2B). All the MC clusters
301 were positive for canonical markers such as *FCER1A* (high-affinity IgE receptor), *MS4A2* (IgE
302 subunit), *CD48* (mast cell receptor), and negative for markers like *ITGAX*
303 (macrophage/dendritic cell marker) (Figure S2A), with distinct differentially expressed genes
304 (DEGs) (Figure S2B). Reactome gene ontology analysis of cluster-specific DEGs revealed
305 enrichment of cholesterol, TNF-α, and TGFβ signaling in LTBI, while oxidative
306 phosphorylation, IFNγ signaling, and MYC signaling were enriched in the PTB group (Figure
307 2C). Plotting the summed *Ucell* module scores revealed significant upregulation of IFNγ
308 signaling, oxidative Phosphorylation, and Th2 signature in PTB ($P < 0.05$), while LTBI and
309 HC clusters showed enhanced TNF-α signaling ($P < 0.05$) (Figure 2D-G; Figure S2 C-F). These
310 results indicate that MCs exhibited distinct transcriptomic profiles depending on the disease
311 state, with MCs from LTBI and HC showing more metabolically active pathways, while MCs
312 from PTB display a more pro-inflammatory signature.

313 Since we observed increased tryptase and chymase in MCs of PTB macaques (Figure 1C), we
314 next examined the levels of tryptase and chymase genes within the single-cell dataset. As we
315 were examining these genes across species, we observed considerable variation in sequence
316 similarity and functional annotation of tryptase genes between humans and NHPs. While
317 *TPSG1* (encoding γ tryptase) and *TPSD1* (encoding δ tryptase) share the gene name in humans
318 and NHPs, the gene corresponding to the more widely expressed *TPSAB1* (encoding α and β1
319 tryptase) differs in NHPs. Based on phylogenetic similarity to human α and β tryptase, the
320 NHP ortholog is often referred to as α-like or β-like (α/β) tryptase. However, their gene names
321 differ, as they are still classified as putative proteins and not formally annotated with the same
322 nomenclature as in humans. The putative tryptase genes in NHPs are annotated as *LOC699599*
323 for *Macaca (M). mulatta* and *LOC102139613* for *M. fasicularis.* Examining these genes in the
324 NHP single cell transcriptome dataset, we detected the expression of the γ and the putative
325 α/βtryptase genes, but found no expression for δ tryptase. *TPSG1* was found to be expressed
326 at low levels and only in a few MCs from the PTB group. In contrast, the putative α/β tryptase
327 gene was expressed in MCs across all groups, with the highest expression in PTB (Figure 2H),
328 consistent with our immunofluorescence data (Figure 1D). As expected, the chymase (encoded
329 by *CMA1*) expressing cells were detected exclusively in the PTB group and were absent in
330 LTBI and HCs (Figure 2H). To confirm whether these *CMA1*-positive cells also co-expressed
331 the putative α/β tryptase as well, we quantified cells expressing single and dual transcripts.
332 This analysis revealed that most of the chymase-positive cells (243 cells) also expressed the
333 putative α/β tryptase gene (183 cells), supporting our earlier observation of a dual tryptase-
334 chymase MC signature linked with PTB. In contrast, MCs from HC and LTBI groups showed
335 expression of tryptase alone (Figure 2I).

336 To strengthen our findings, we validated MCs using an independent lung single-cell
337 transcriptome from NHP (*M. fasicularis*), collected at 4 weeks (higher bacterial load, more
338 severe disease) and 10 weeks (low bacterial load, less severe disease) following low-dose *Mtb*
339 Erdman infection (Gideon et al., 2022; Grimbaldeston et al., 2005). This dataset had 372 MCs
340 at 4 weeks, and 7306 MCs at 10 weeks (Figure 2J). We examined the expression of chymase
341 and several tryptase genes, including *TPSG1*, *TPSD1*, and *LOC102140229* (putative NHP
342 ortholog for human *TPSAB1*). While *TPSD1* expression was undetectable, the other tryptase
343 genes showed high expression with a pronounced increase in chymase (*CMA1*) expression both
344 at 4 and 10 weeks (Figure 2K). Similar to our transcriptomic scRNA seq dataset, we quantified
345 MCs co-expressing *LOC102140229* and *CMA1*. Consistent with our data, *CMA1* and
346 *LOC102140229* (the α/β-like tryptase ortholog) expressions were associated with severe
347 disease, being significantly enriched in MCs from the higher-burden 4-week granulomas, (OR
348 = 0.27, $p < 1\times10^{-29}$, and OR = 1.68, $p < 1\times10^{-5}$, respectively). Importantly, when restricting
349 analysis to *CMA1*$^{+}$ cells, the dual-positive *CMA1*$^{+}$*LOC102140229*$^{+}$ MC subset was
350 proportionally more abundant in less severe, 10-week granulomas (OR = 0.51, $p < 1\times10^{-9}$)
351 (Figure 2M). This suggested that while chymase (*CMA1*) expression marked severe disease,
352 the presence of the dual tryptase–chymase phenotype in less severe lesions, supported the idea
353 that MC transcriptional diversity emerges in association with disease modulation This further
354 supporting our observation of MC diversity with increasing dual tryptase and chymase
355 signature associated with disease progression. Similar to our observations in *M. mulatta*, we
356 quantified the DEGs and carried out Ucell scores in the MC subset from *M. fascicularis* .We
357 observed that MC from high burden TB granulomas showed higher IFNγ signaling, oxidative
358 phosphorylation (Figure 2N-O), similar to higher PTB scores seen in *M. mulatta*. However,
359 unlike *M. mulatta*, *M. fascicularis* also showed increased TNF signaling in high-burden
360 granulomas (Figure 2P). These results highlight that MCs in high-burden granulomas

361 upregulated IFNγ, TNF, and metabolic programs, coupled with chymase expression, whereas
362 less severe granulomas were enriched for tryptase-positive MCs. Although this mirrors our
363 findings seen in in *M. mulatta*, we observed species-specific differences in how TNF signaling
364 is distributed across disease states.

365 **MC-deficient mice exhibit enhanced control of *Mtb***

366 We next determined whether MCs are induced in response to *Mtb* infection in mice, and
367 characterized their accumulation early and later in infection. In our previous studies, we
368 observed that innate cells such as innate lymphoid cells (ILCs) accumulate rapidly between
369 days 5-10 post-infection, followed by neutrophils, macrophages, and monocytes between days
370 10-15, and T cells by days 21 to 30 (Ardain et al., 2019). We found that MCs begin to
371 accumulate in the lungs between days 21 and 30, coinciding with the timing of *Mtb* growth
372 (Figure S3A-B) and T cell recruitment. To investigate the functional role of MCs in *Mtb*
373 infection, we utilized the MC-deficient mouse model, *CgKitW*^{sh}. These mice carry spontaneous
374 loss-of-function mutations in both alleles of the dominant *white spotting* (*W*) locus (*i.e.*, c-*kit*),
375 leading to impaired c-*kit* tyrosine kinase-dependent signaling resulting in dysregulated MC
376 development, survival, and function (Wolters et al., 2005). We infected *CgKitW*^{sh} mice with
377 low-dose aerosolized *Mtb* strain HN878 for early (50 days post infection, dpi) and later time
378 points (100 dpi and 150 dpi) and compared them with C57BL/6 wild-type (WT) *Mtb*-infected
379 mice (Figure 3A). While there were no significant differences observed in lung and spleen
380 bacterial burden at 50 dpi between *CgKitW*^{sh} and WT *Mtb*-infected mice, *CgKitW*^{sh} *Mtb*-
381 infected mice showed significantly lower lung and spleen *Mtb* CFU compared to WT *Mtb*-
382 infected controls at 100 dpi. However, at 150 dpi, lung bacterial burden in *CgKitW*^{sh} *Mtb*-
383 infected mice trended lower but not significant, these mice showed enhanced bacterial control
384 in the spleen (Figure 3B-C). The reduction in bacterial load also coincided with reduced lung
385 inflammation in *CgKitW*^{sh} *Mtb*-infected mice at 150 dpi (Figure 3D-E). These findings indicate

386 that MC-deficient *CgKitW*^{sh} mice exhibit improved control of *Mtb* infection during chronic
387 stages, suggesting that MCs may contribute to disease persistence or pathogenesis in chronic
388 TB.
389

390 **MC-deficient mice display altered innate immune cell profiles during chronic *Mtb***
391 **infection**

392 To further address the functional basis of enhanced protection observed in MC-deficient mice,
393 we analyzed the lung immune responses in *CgKitW*^{sh} mice both at baselines and following *Mtb*
394 infection, given that this mouse strain is associated with other known immune alterations
395 (Grimbaldeston et al., 2005). MCs were significantly reduced in the lungs of *CgKitW*^{sh} mice
396 compared to WT mice at baseline (Figure 4A). However, we did not observe any significant
397 differences in other innate immune populations in the lung of *CgKitW*^{sh} mice, including
398 dendritic cells (DCs), recruited macrophages (RMs), alveolar macrophages (AMs),
399 neutrophils, monocytes, and T cells at baseline compared to WT controls (Figure 4B-F and
400 S4). Following *Mtb* infection, MCs accumulated progressively in the lungs of both WT and
401 *CgKitW*^{sh} mice up to 100 dpi, after which their numbers stabilized through 150 dpi. In contrast,
402 MC accumulation was significantly impaired in *CgKitW*^{sh} mice throughout infection (Figure
403 4A). At 50 dpi, RMs were elevated in *CgKitW*^{sh} mice, with no significant difference observed
404 in DCs or neutrophils compared to WT mice (Figure 4B). By 100 dpi, both DCs and neutrophils
405 were decreased in *CgKitW*^{sh} mice; however, these changes were not sustained at 150 dpi
406 (Figure 4C-D). Across all time points, AMs and monocyte populations remained comparable
407 between *CgKitW*^{sh} and WT *Mtb*-infected mice (Figure 4E-F). Previous studies have implicated
408 MCs in driving T cell responses (Elieh Ali Komi & Grauwet, 2018), therefore, we next
409 examined T cell responses induced post-infection. We found no differences in the activated
410 $CD4^+$ and $CD8^+$ T cell responses at 50 dpi however, by 100 dpi, both populations were
411 significantly reduced at 100 dpi in *CgKitW*^{sh} *Mtb*-infected mice (Figure S5A and E). This

412 reduction extended to functional subsets, with fewer $CD4^+$ T cells producing IFNγ, as well as
413 diminished dual TNF-α and IFNγ producing cells in the *CgKitW*^{sh} *Mtb*-infected mice as
414 compared to WT *Mtb*-infected mice (Figure S5B-D). We did not find any significant
415 differences in the $CD8^+$ T cells producing IFNγ, TNF-α, and dual IFNγ and TNF-α producing
416 cells in the *CgKitW*^{sh} *Mtb*-infected mice (Figure S5F-H). Finally, we measured cytokine
417 responses in the lungs of *CgKitW*^{sh} and WT *Mtb*-infected mice at 150 dpi. We found that pro-
418 inflammatory cytokines that direct monocyte/macrophage and T cell responses (G-CSF, IFNγ,
419 IL-1β, IL-6, IL-17, MCP-1, TNF-α, and RANTES) were significantly lower in *CgKitW*^{sh} *Mtb*-
420 infected lungs compared to WT *Mtb*-infected lungs. Similarly, chemokines driving neutrophil
421 recruitment (MIP-1β, and MIP-2) were reduced in *CgKitW*^{sh} *Mtb*-infected mice, whereas Th2
422 cytokines such as IL-13 did not differ between the two groups (Figure 4G). Together, these
423 results provide evidence that MCs are induced following *Mtb* infection, accumulate in the lung,
424 and mediate immune responses that drive pathology and promote *Mtb* susceptibility and
425 dissemination during chronic TB.
426
427 **Transfer of MCs into lung airways promotes neutrophil accumulation and *Mtb***
428 **dissemination.**
429 To examine whether MCs can impact *Mtb* control and dissemination, we adoptively transferred
430 bone marrow-derived MCs into the airways of WT mice, hereafter referred to as $B6^{MC}$ mice.
431 A total of $5x10^4$ MCs were transferred, approximating the number of MCs present in the lungs
432 of WT *Mtb*-infected mice at 100 dpi. Following transfer, mice were infected with *Mtb,* and
433 we found that MCs were retained in the lungs of $B6^{MC}$ *Mtb*-infected mice up to 30 dpi (Figure
434 5A). Strikingly, $B6^{MC}$ *Mtb*-infected mice showed increased neutrophils frequencies and
435 reduced RMs when compared with B6 *Mtb*-infected mice (Figure 5B, and C). However, no
436 differences in the total numbers of lung MCs, neutrophils, RMs or DCs were observed in B6

437 and $B6^{MC}$ groups (Figure S6). While the presence of additional MCs in the lungs did not alter
438 the bacterial burden (*Mtb* CFU) and inflammation in the lungs, $B6^{MC}$ *Mtb*-infected mice
439 showed a significant increase in the *Mtb* CFUs in the spleen, suggesting a role for MCs in
440 promoting dissemination from the lungs (Figure 5D-F). Consistently, histological analysis
441 revealed greater neutrophil infiltration in lung sections of $B6^{MC}$ *Mtb*-infected mice compared
442 to WT *Mtb*-infected mice (Figure 5G and H), implicating MCs in driving neutrophil
443 recruitment and potentially enhancing the systemic spread of *Mtb*.
444

445 **Discussion**

446 The immune mechanism(s) that mediate the progression from LTBI to PTB are unclear. In this
447 study, we identified MCs as an innate cell type that is overrepresented during PTB,
448 transcriptionally expressed signatures associated with IFNγ, oxidative phosphorylation, and
449 MYC signaling, and localized within mature TB granulomas. Importantly, using mice deficient
450 in MCs, we showed a potential pathological role for MCs in mediating susceptibility to TB,
451 thus providing MCs as a novel therapeutic target.
452 MCs have been shown to interact with *Mtb* through the GPI-anchored molecule CD48 (Munoz
453 et al., 2003), interaction with TLR2 (Carlos et al., 2007), and potentially TLR4 (McCurdy et
454 al., 2001). Additionally, *Mtb* is also thought to be internalized by lipid rafts on MCs (Munoz
455 et al., 2009), thus serving as a long-lasting reservoir for *Mtb* (da Silva et al., 2014). These in
456 vitro studies have shown that MC exposure to *Mtb* results in degranulation of MCs, as well as
457 the induction of proinflammatory cytokines such as TNF-α and IL-1β. Consistently, another
458 study using the same route of high-dose infection reported increased bacterial burden in both
459 the lungs and spleen of MC-deficient Kit^W-sh/W-sh mice compared to wild-type C57BL/6
460 controls (Villareal-Rivota et al., 2025). While these studies using a high-dose model of
461 infection reported early induction of inflammatory mediators from MC within hours to days,

462 our in vivo results using a physiological low dose of *Mtb* infection model showed that MCs
463 accumulated between 21-30 days, coinciding with the onset of T cells in the lung. Interestingly,
464 despite the accumulation of MCs in the lung at 30 dpi following low-dose aerosol infection,
465 the impact of MC deficiency on *Mtb* control and inflammation in *CgKitW*^{sh} mice was not
466 evident until 100 dpi. This is similar to our published studies where we found that S100A8/9
467 deficiency resulted in reduced neutrophil lung accumulation (Scott et al., 2020), resulting in
468 improved *Mtb* control and improved TB disease, but after 100 dpi. However, this is in contrast
469 to the role of eosinophils in TB, as eosinophil deficiency resulted in increased *Mtb* CFU
470 (Bohrer et al., 2021). MCs were the primary innate cell type that were defective in the lungs
471 of *CgKitW*^{sh} mice at baseline and throughout infection, and their absence was associated with
472 better containment of *Mtb* in both lung and spleen, indicating a pathological role for MCs
473 during chronic TB.
474 Our data also showed that MCs accumulated in the lungs of C57BL/6 mice from 50 to 100 dpi,
475 after which their numbers stabilized. This increased accumulation of MCs during chronic
476 infection coincided with elevated infiltration of DCs and neutrophils. Importantly, we showed
477 that enhancing MCs numbers through adoptive transfer in the lungs of WT *Mtb*-infected mice
478 similarly promoted neutrophil accumulation and facilitated *Mtb* dissemination. This suggests
479 that MCs are not merely a consequence of chronic inflammation, but active modulators capable
480 of shaping immune cell dynamics early in infection. When present in sufficient numbers, MCs
481 with their ability to promote neutrophil recruitment, can potentially influence the balance of
482 protective versus pathological inflammation during TB. These results raise the possibility that
483 MC accumulation during chronic infection serves to fine-tune the composition of the innate
484 immune compartment in the lung. Whether this regulation is beneficial or detrimental to host
485 control of *Mtb* remains to be explored. However, our data suggested that manipulating MC
486 responses may offer a novel avenue for modulating immune dynamics in TB, particularly in

487 the chronic phase, where inflammation must be tightly regulated to prevent tissue damage.
488 Additionally, the reduced inflammation observed at 150 dpi is associated with decreased levels
489 of proinflammatory cytokines and chemokines that recruit monocytes/macrophages, and T
490 cells, and neutrophils. Overall, based on our results along with the current literature, we
491 propose pathological roles for neutrophils and MCs, while other granulocytes, such as
492 eosinophils, may mediate protective roles (Bohrer et al., 2021).
493 MCs can release cytokines and chemokines, antimicrobial peptides, and granules upon
494 pathogen sensing and to control pathogens (Naqvi et al., 2017; Naqvi et al., 2021; Naqvi et al.,
495 2020). In the context of *Mtb* exposure, MCs have been shown to undergo degranulation,
496 including histamine and β-hexosaminidase (Munoz et al., 2003). Indeed, histamine-deficient
497 mice showed decreased neutrophils, as well as proinflammatory cytokine production following
498 *Mtb* infection (Carlos et al., 2009). Additionally, induction of degranulation following
499 intratracheal *Mtb* infection resulted in reduced proinflammatory cytokines as well as reduced
500 lung inflammation. Similarly, our study showed reduced DCs, neutrophils, and $CD4^+$ and $CD8^+$
501 T cell responses, in the lungs of MC-deficient *Mtb*-infected mice, along with reduced
502 proinflammatory cytokines and lung inflammation at chronic time points. Thus, together with
503 published work, MCs can potentially modulate neutrophils and other inflammatory mediators
504 in high-dose models, as well as in a physiologically relevant *Mtb* infection model, leading to
505 disease pathology. The exact mechanism by which MCs contribute to the pathology,
506 dissemination, and promote *Mtb* infection is an area of future investigation.
507 At baseline, human lungs have been reported to primarily express tryptase (Poto et al., 2022).
508 Indeed, we found that this is true for both macaque and human lungs in our study, where healthy
509 lungs expressed MC_Ts. Additionally, we found that early granulomas and in LTBI we saw
510 expression of MC_{TC}s with a switch to more and accumulation of MC_Cs in late-stage
511 granulomas. Chymase expression may modulate extracellular matrix components (ECM) such

512 as fibronectin, leading to tissue remodeling, impacting cellular communication, and inducing
513 cleavage for key cytokines such as IL-6, IL-13, IL-15, and IL-33, as well as TGF-β. (Pejler,
514 2020; Waern et al., 2013). Studies have shown that tryptase can induce proliferation of
515 fibroblasts, epithelial cells, and smooth muscle cells, causing airway remodeling during
516 diseased conditions (Mogren et al., 2021). Tryptase can also inactivate a large range of peptides
517 by cleaving specific substrates, such as fibrinogen, gelatin, pro-matrix metalloproteinases
518 (MMP), and complement factors, thus moderating inflammatory responses (Caughey, 2007).
519 Based on our results from human and macaque lung, we hypothesize that MC_{TC}s may synergize
520 to drive responses induced by both pathways at early time points and possibly just by MC_{C}s at
521 later time points. Additional studies describing these subsets and testing their functional
522 relevance in *in vivo* models are future steps in delineating the role of these subsets in TB.
523 Single-cell transcriptomic analysis revealed a differential activation state between the MCs that
524 accumulate in lungs in PTB as compared to LTBI and HC in NHPs (Esaulova et al., 2021).
525 The MCs from PTB animals showed a closer resemblance to MC_{CS}, characterized by higher
526 IFNγ, metabolic activation, and chymase signatures, confirming that chymase expression is
527 associated with disease severity. This association of chymase expression with disease severity
528 was confirmed in an independent single-cell lung dataset (Gideon et al., 2022), where the
529 analysis revealed similar enrichment of chymase-expressing MC_{C}s in granulomas with higher
530 disease burden, accompanied by similar activation of IFN-γ and metabolic pathways.
531 Metabolic activation of oxidative phosphorylation, as observed here, has been associated with
532 activated MCs, and inhibiting mitochondrial ATP production reduced MC degranulation and
533 cytokine production (Paruchuru et al., 2022; Sharkia et al., 2017). This also suggests that MCs,
534 which accumulate in the lungs in LTBI and HC, were not only lower in proportion but also less
535 activated, meaning that TB-induced activation of MCs contributes to their pathogenic
536 phenotype in disease. Our data aligned with previous observations by Garcia-Rodriguez *et al.*,

537 2021, showing that chymase-expressing MCs accumulate in TB-induced lung lesions and may
538 contribute to fibrotic processes surrounding granulomas (Garcia-Rodriguez et al., 2021). We
539 also observed an expansion of MC_{TC}s in the PTB group in NHPs, mirroring the phenotypic
540 shift from M_{CT} to MC_{TC} seen in human lung sections. While Garcia-Rodriguez *et al*. suggested
541 this shift occurs in fibrotic areas and may reflect tissue remodeling, they did not demonstrate
542 improved lung function. Although fibrosis was not directly measured in our study, these
543 findings support the association of chymase-positive MCs with advanced, inflammatory
544 disease, reinforcing their potential role in TB pathogenesis.
545 MCs are known to gear towards a Th2 signature with increased chymase expression (Toru et
546 al., 1998). This increase was reflected in MCs from the macaque lung, showing a high
547 transcriptomic Th2 signature in PTB but not in clusters found in LTBI and HC. In essence,
548 transcriptomics reflected the hyperactivated nature of the MCs in PTB, which might make them
549 more pathological during infection. Although our *in vivo* mouse study showed a pathological
550 role of MCs, significant secretion of Th2 cytokines was not seen, likely because the C57Bl/6
551 mouse model is prone towards Th1 polarization (Wakeham et al., 2000). MCs can release both
552 preformed and de novo synthesized TNF-α, hence helping in early bacterial clearance (Gordon
553 & Galli, 1991). Similarly, our study showed that the MCs from HC and LTBI individuals
554 expressed higher levels of TNF-α and were in a less metabolically activated state (lower
555 OXPHOS signature). So, additional studies will help in elucidating the mechanism through
556 which MCs mediate pathological roles.
557 In summary, we demonstrated that the accumulation of chymase-producing MCs in PTB is a
558 cross-species phenomenon that contributes to increased TB pathology and loss of TB control,
559 thereby elucidating the pathological role of MCs in the control of *Mtb* infection. By targeting
560 MC pathways or signaling mechanisms, host-directed therapies (HDTs) hold the promise of

561 enhancing the effectiveness of existing treatments and mitigating disease-related
562 complications.
563

564 **Acknowledgements**

565 This work was supported by Washington University in St. Louis; NIH grants HL105427,
566 AI111914, AI134236, and AI123780 to S.A.K., and the Department of Microbiology,
567 University of Chicago. We thank Ms. Lan Lu, Washington University in St. Louis, and Adlai
568 Politi, University of Chicago, for technical support and assistance.
569

570 **Authors Contributions**

571 S.A.K. supervised all aspects of the study. A.G. and V.T. share co-authorship. A.G., V.T.
572 designed, performed experiments, and analyzed data. A.G., V.T., and A.A. constructed figures
573 and analyzed data. J.R.M., N.N., Y.T., M.A., and K.S.C. curated data/contributed resources
574 and/or data analysis. A.G., V.T., and S.A.K. wrote the original draft of the manuscript. S.A.K.,
575 A.G., V.T., A.A., and N.N. reviewed and edited the manuscript. J.Z. provided the human
576 specimens. D.K. provided the NHP specimen, and D.K. and S.A.K. provided funding. All
577 authors reviewed, edited, and approved the manuscript.
578

579 **Competing interests.**

580 The authors declare no competing interests.
581

582 **References**

583 Ardain, A., Domingo-Gonzalez, R., Das, S., Kazer, S. W., Howard, N. C., Singh, A., Ahmed,
584 M., Nhamoyebonde, S., Rangel-Moreno, J., Ogongo, P., Lu, L., Ramsuran, D., de la
585 Luz Garcia-Hernandez, M., T, K. U., Darby, M., Park, E., Karim, F., Melocchi, L.,
586 Madansein, R., . . . Khader, S. A. (2019). Group 3 innate lymphoid cells mediate early
587 protective immunity against tuberculosis. *Nature*, *570*(7762), 528-532.
588 https://doi.org/10.1038/s41586-019-1276-2
589 Bian, G., Gu, Y., Xu, C., Yang, W., Pan, X., Chen, Y., Lai, M., Zhou, Y., Dong, Y., Mao, B.,
590 Zhou, Q., Chen, B., Nakathata, T., Shi, L., Wu, M., Zhang, Y., & Ma, F. (2021). Early
591 development and functional properties of tryptase/chymase double-positive mast cells
592 from human pluripotent stem cells. *J Mol Cell Biol*, *13*(2), 104-115.
593 https://doi.org/10.1093/jmcb/mjaa059
594 Bohrer, A. C., Castro, E., Hu, Z., Queiroz, A. T. L., Tocheny, C. E., Assmann, M., Sakai, S.,
595 Nelson, C., Baker, P. J., Ma, H., Wang, L., Zilu, W., du Bruyn, E., Riou, C.,
596 Kauffman, K. D., Tuberculosis Imaging, P., Moore, I. N., Del Nonno, F., Petrone, L.,
597 . . . Mayer-Barber, K. D. (2021). Eosinophils are part of the granulocyte response in
598 tuberculosis and promote host resistance in mice. *J Exp Med*, *218*(10).
599 https://doi.org/10.1084/jem.20210469
600 Carlos, D., de Souza Junior, D. A., de Paula, L., Jamur, M. C., Oliver, C., Ramos, S. G.,
601 Silva, C. L., & Faccioli, L. H. (2007). Mast cells modulate pulmonary acute
602 inflammation and host defense in a murine model of tuberculosis. *J Infect Dis*, *196*(9),
603 1361-1368. https://doi.org/10.1086/521830
604 Carlos, D., Fremond, C., Samarina, A., Vasseur, V., Maillet, I., Ramos, S. G., Erard, F.,
605 Quesniaux, V., Ohtsu, H., Silva, C. L., Faccioli, L. H., & Ryffel, B. (2009). Histamine
606 plays an essential regulatory role in lung inflammation and protective immunity in the
607 acute phase of Mycobacterium tuberculosis infection. *Infect Immun*, *77*(12), 5359-
608 5368. https://doi.org/10.1128/IAI.01497-08
609 Caughey, G. H. (2007). Mast cell tryptases and chymases in inflammation and host defense.
610 *Immunol Rev*, *217*, 141-154. https://doi.org/10.1111/j.1600-065X.2007.00509.x
611 da Silva, E. Z., Jamur, M. C., & Oliver, C. (2014). Mast cell function: a new vision of an old
612 cell. *J Histochem Cytochem*, *62*(10), 698-738.
613 https://doi.org/10.1369/0022155414545334
614 Elieh Ali Komi, D., & Grauwet, K. (2018). Role of Mast Cells in Regulation of T Cell
615 Responses in Experimental and Clinical Settings. *Clin Rev Allergy Immunol*, *54*(3),
616 432-445. https://doi.org/10.1007/s12016-017-8646-z
617 Esaulova, E., Das, S., Singh, D. K., Choreno-Parra, J. A., Swain, A., Arthur, L., Rangel-
618 Moreno, J., Ahmed, M., Singh, B., Gupta, A., Fernandez-Lopez, L. A., de la Luz
619 Garcia-Hernandez, M., Bucsan, A., Moodley, C., Mehra, S., Garcia-Latorre, E.,
620 Zuniga, J., Atkinson, J., Kaushal, D., . . . Khader, S. A. (2021). The immune
621 landscape in tuberculosis reveals populations linked to disease and latency. *Cell Host*
622 *Microbe*, *29*(2), 165-178 e168. https://doi.org/10.1016/j.chom.2020.11.013
623 Garcia-Rodriguez, K. M., Bini, E. I., Gamboa-Dominguez, A., Espitia-Pinzon, C. I., Huerta-
624 Yepez, S., Bulfone-Paus, S., & Hernandez-Pando, R. (2021). Differential mast cell
625 numbers and characteristics in human tuberculosis pulmonary lesions. *Sci Rep*, *11*(1),
626 10687. https://doi.org/10.1038/s41598-021-89659-6
627 Gideon, H. P., Hughes, T. K., Tzouanas, C. N., Wadsworth, M. H., 2nd, Tu, A. A., Gierahn,
628 T. M., Peters, J. M., Hopkins, F. F., Wei, J. R., Kummerlowe, C., Grant, N. L.,
629 Nargan, K., Phuah, J. Y., Borish, H. J., Maiello, P., White, A. G., Winchell, C. G.,
630 Nyquist, S. K., Ganchua, S. K. C., . . . Shalek, A. K. (2022). Multimodal profiling of

631 lung granulomas in macaques reveals cellular correlates of tuberculosis control.
632 *Immunity*, *55*(5), 827-846 e810. https://doi.org/10.1016/j.immuni.2022.04.004
633 Gopal, R., Rangel-Moreno, J., Slight, S., Lin, Y., Nawar, H. F., Fallert Junecko, B. A.,
634 Reinhart, T. A., Kolls, J., Randall, T. D., Connell, T. D., & Khader, S. A. (2013).
635 Interleukin-17-dependent CXCL13 mediates mucosal vaccine-induced immunity
636 against tuberculosis. *Mucosal Immunol*, *6*(5), 972-984.
637 https://doi.org/10.1038/mi.2012.135
638 Gordon, J. R., & Galli, S. J. (1991). Release of both preformed and newly synthesized tumor
639 necrosis factor alpha (TNF-alpha)/cachectin by mouse mast cells stimulated via the Fc
640 epsilon RI. A mechanism for the sustained action of mast cell-derived TNF-alpha
641 during IgE-dependent biological responses. *J Exp Med*, *174*(1), 103-107.
642 https://doi.org/10.1084/jem.174.1.103
643 Griffiths, K. L., Ahmed, M., Das, S., Gopal, R., Horne, W., Connell, T. D., Moynihan, K. D.,
644 Kolls, J. K., Irvine, D. J., Artyomov, M. N., Rangel-Moreno, J., & Khader, S. A.
645 (2016). Targeting dendritic cells to accelerate T-cell activation overcomes a
646 bottleneck in tuberculosis vaccine efficacy. *Nat Commun*, *7*, 13894.
647 https://doi.org/10.1038/ncomms13894
648 Grimbaldeston, M. A., Chen, C. C., Piliponsky, A. M., Tsai, M., Tam, S. Y., & Galli, S. J.
649 (2005). Mast cell-deficient W-sash c-kit mutant Kit W-sh/W-sh mice as a model for
650 investigating mast cell biology in vivo. *Am J Pathol*, *167*(3), 835-848.
651 https://doi.org/10.1016/S0002-9440(10)62055-X
652 Kaushal, D., Foreman, T. W., Gautam, U. S., Alvarez, X., Adekambi, T., Rangel-Moreno, J.,
653 Golden, N. A., Johnson, A. M., Phillips, B. L., Ahsan, M. H., Russell-Lodrigue, K. E.,
654 Doyle, L. A., Roy, C. J., Didier, P. J., Blanchard, J. L., Rengarajan, J., Lackner, A. A.,
655 Khader, S. A., & Mehra, S. (2015). Mucosal vaccination with attenuated
656 Mycobacterium tuberculosis induces strong central memory responses and protects
657 against tuberculosis. *Nat Commun*, *6*, 8533. https://doi.org/10.1038/ncomms9533
658 Khader, S. A., Bell, G. K., Pearl, J. E., Fountain, J. J., Rangel-Moreno, J., Cilley, G. E., Shen,
659 F., Eaton, S. M., Gaffen, S. L., Swain, S. L., Locksley, R. M., Haynes, L., Randall, T.
660 D., & Cooper, A. M. (2007). IL-23 and IL-17 in the establishment of protective
661 pulmonary CD4+ T cell responses after vaccination and during Mycobacterium
662 tuberculosis challenge. *Nat Immunol*, *8*(4), 369-377. https://doi.org/10.1038/ni1449
663 McCurdy, J. D., Lin, T. J., & Marshall, J. S. (2001). Toll-like receptor 4-mediated activation
664 of murine mast cells. *J Leukoc Biol*, *70*(6), 977-984.
665 https://www.ncbi.nlm.nih.gov/pubmed/11739561
666 Mogren, S., Berlin, F., Ramu, S., Sverrild, A., Porsbjerg, C., Uller, L., & Andersson, C. K.
667 (2021). Mast cell tryptase enhances wound healing by promoting migration in human
668 bronchial epithelial cells. *Cell Adh Migr*, *15*(1), 202-214.
669 https://doi.org/10.1080/19336918.2021.1950594
670 Munoz, S., Hernandez-Pando, R., Abraham, S. N., & Enciso, J. A. (2003). Mast cell
671 activation by Mycobacterium tuberculosis: mediator release and role of CD48. *J*
672 *Immunol*, *170*(11), 5590-5596. https://doi.org/10.4049/jimmunol.170.11.5590
673 Munoz, S., Rivas-Santiago, B., & Enciso, J. A. (2009). Mycobacterium tuberculosis entry
674 into mast cells through cholesterol-rich membrane microdomains. *Scand J Immunol*,
675 *70*(3), 256-263. https://doi.org/10.1111/j.1365-3083.2009.02295.x
676 Naqvi, N., Ahuja, K., Selvapandiyan, A., Dey, R., Nakhasi, H., & Puri, N. (2017). Role of
677 Mast Cells in clearance of Leishmania through extracellular trap formation. *Sci Rep*,
678 *7*(1), 13240. https://doi.org/10.1038/s41598-017-12753-1
679 Naqvi, N., Srivastava, R., Naskar, P., & Puri, N. (2021). Mast cells modulate early responses
680 to Mycobacterium bovis Bacillus Calmette-Guerin by phagocytosis and formation of

681 extracellular traps. *Cell Immunol*, *365*, 104380.
682 https://doi.org/10.1016/j.cellimm.2021.104380
683 Naqvi, N., Srivastava, R., Selvapandiyan, A., & Puri, N. (2020). Host Mast Cells in
684 Leishmaniasis: Friend or Foe? *Trends Parasitol*, *36*(12), 952-956.
685 https://doi.org/10.1016/j.pt.2020.09.010
686 Paruchuru, L. B., Govindaraj, S., & Razin, E. (2022). The Critical Role Played by
687 Mitochondrial MITF Serine 73 Phosphorylation in Immunologically Activated Mast
688 Cells. *Cells*, *11*(3). https://doi.org/10.3390/cells11030589
689 Pejler, G. (2020). Novel Insight into the in vivo Function of Mast Cell Chymase: Lessons
690 from Knockouts and Inhibitors. *J Innate Immun*, *12*(5), 357-372.
691 https://doi.org/10.1159/000506985
692 Poto, R., Criscuolo, G., Marone, G., Brightling, C. E., & Varricchi, G. (2022). Human Lung
693 Mast Cells: Therapeutic Implications in Asthma. *Int J Mol Sci*, *23*(22).
694 https://doi.org/10.3390/ijms232214466
695 Scott, N. R., Swanson, R. V., Al-Hammadi, N., Domingo-Gonzalez, R., Rangel-Moreno, J.,
696 Kriel, B. A., Bucsan, A. N., Das, S., Ahmed, M., Mehra, S., Treerat, P., Cruz-
697 Lagunas, A., Jimenez-Alvarez, L., Munoz-Torrico, M., Bobadilla-Lozoya, K., Vogl,
698 T., Walzl, G., du Plessis, N., Kaushal, D., . . . Khader, S. A. (2020). S100A8/A9
699 regulates CD11b expression and neutrophil recruitment during chronic tuberculosis. *J*
700 *Clin Invest*, *130*(6), 3098-3112. https://doi.org/10.1172/JCI130546
701 Sharan, R., Singh, D. K., Rengarajan, J., & Kaushal, D. (2021). Characterizing Early T Cell
702 Responses in Nonhuman Primate Model of Tuberculosis. *Front Immunol*, *12*, 706723.
703 https://doi.org/10.3389/fimmu.2021.706723
704 Sharkia, I., Hadad Erlich, T., Landolina, N., Assayag, M., Motzik, A., Rachmin, I., Kay, G.,
705 Porat, Z., Tshori, S., Berkman, N., Levi-Schaffer, F., & Razin, E. (2017). Pyruvate
706 dehydrogenase has a major role in mast cell function, and its activity is regulated by
707 mitochondrial microphthalmia transcription factor. *J Allergy Clin Immunol*, *140*(1),
708 204-214 e208. https://doi.org/10.1016/j.jaci.2016.09.047
709 Singh, D. K., Ahmed, M., Akter, S., Shivanna, V., Bucsan, A. N., Mishra, A., Golden, N. A.,
710 Didier, P. J., Doyle, L. A., Hall-Ursone, S., Roy, C. J., Arora, G., Dick, E. J., Jr.,
711 Jagannath, C., Mehra, S., Khader, S. A., & Kaushal, D. (2025). Prevention of
712 tuberculosis in cynomolgus macaques by an attenuated Mycobacterium tuberculosis
713 vaccine candidate. *Nat Commun*, *16*(1), 1957. https://doi.org/10.1038/s41467-025-
714 57090-4
715 Toru, H., Eguchi, M., Matsumoto, R., Yanagida, M., Yata, J., & Nakahata, T. (1998).
716 Interleukin-4 promotes the development of tryptase and chymase double-positive
717 human mast cells accompanied by cell maturation. *Blood*, *91*(1), 187-195.
718 https://www.ncbi.nlm.nih.gov/pubmed/9414284
719 Varma, R., & Puri, N. (2019). Dampening of mast cell secondary responses to allergen
720 involves specific signalling and epigenetic changes. *Cell Immunol*, *344*, 103944.
721 https://doi.org/10.1016/j.cellimm.2019.103944
722 Villareal-Rivota, B., Meneses-Preza, Y. G., Campillo-Navarro, M., Ruiz-Sanchez, B. P.,
723 Soria-Castro, R., Barrios-Payan, J., Mata-Espinosa, D., Donis-Maturano, L., Perez-
724 Tapia, S. M., Chavez-Blanco, A. D., Estrada-Parra, S., Hernandez-Pando, R., &
725 Chacon-Salinas, R. (2025). Impaired control of Mycobacterium tuberculosis infection
726 in mast cell-deficient Kit(W-sh/W-sh) mice. *Tuberculosis (Edinb)*, *150*, 102587.
727 https://doi.org/10.1016/j.tube.2024.102587
728 Virk, H., Arthur, G., & Bradding, P. (2016). Mast cells and their activation in lung disease.
729 *Transl Res*, *174*, 60-76. https://doi.org/10.1016/j.trsl.2016.01.005

730 Waern, I., Lundequist, A., Pejler, G., & Wernersson, S. (2013). Mast cell chymase modulates
731 IL-33 levels and controls allergic sensitization in dust-mite induced airway
732 inflammation. *Mucosal Immunol*, *6*(5), 911-920. https://doi.org/10.1038/mi.2012.129
733 Wakeham, J., Wang, J., & Xing, Z. (2000). Genetically determined disparate innate and
734 adaptive cell-mediated immune responses to pulmonary Mycobacterium bovis BCG
735 infection in C57BL/6 and BALB/c mice. *Infect Immun*, *68*(12), 6946-6953.
736 https://doi.org/10.1128/IAI.68.12.6946-6953.2000
737 Wasserman, S. I. (1984). The human lung mast cell. *Environ Health Perspect*, *55*, 259-269.
738 https://doi.org/10.1289/ehp.8455259
739 WHO. (2024). *Global Tuberculosis Report*.
740 Wolters, P. J., Mallen-St Clair, J., Lewis, C. C., Villalta, S. A., Baluk, P., Erle, D. J., &
741 Caughey, G. H. (2005). Tissue-selective mast cell reconstitution and differential lung
742 gene expression in mast cell-deficient Kit(W-sh)/Kit(W-sh) sash mice. *Clin Exp*
743 *Allergy*, *35*(1), 82-88. https://doi.org/10.1111/j.1365-2222.2005.02136.x
744

745

746 **Figure legends**

747 **Figure 1. Chymase positive MCs are predominant in TB infected human and macaque**
748 **lung tissue.** Lung biopsies from healthy individuals (n = 4) or patients with PTB (n = 5) were
749 stained for tryptase MC_T (green) or chymase MC_C (red). (A) Immunofluorescence microscopy
750 shows MC_{TS} (green) in healthy lung biopsies (HC). MC_{TCS} (red and green merge) are located
751 around the early granulomas, while MC_{CS} (red) surround the late granulomas in TB infected
752 lung biopsies. (B) Predominance of MC_{TS} in healthy lungs transitioning to MC_{TCS} in early
753 granuloma and becoming MC_{CS} in late granulomas in TB infected lungs. (C)
754 Immunofluorescence microscopy shows MC_{TS} (green) and MC_{TCS} (merge) in lungs of healthy
755 (HC), LTBI and PTB macaques. (D) Predominance of MC_{TS} (green) and MC_{TCS} (merge) in
756 PTB compared to LTBI and HC. Statistical analysis was performed using unpaired, 2-tailed
757 Student's t test, **** $p < 0.0001$, *** $p < 0.001$, * $p< 0.05$.

758

759 **Figure 2. MC signatures across disease conditions in NHPs.** Data was re-analyzed from the
760 lungs of *M. mulatta* infected with *Mtb CDC1551* (GSE200151). (A) Schematic of the study
761 design across disease conditions (B) UMAP embedding of *FCER1A*+ mast cells, showing the
762 distribution of these cells across the different disease conditions (PTB in pink, HC in green,
763 and LTBI in blue). (C) Heatmap of Hallmark pathway analysis for differentially expressed
764 genes, highlighting the top pathways with the highest FDR values for each condition. (D-G)
765 UCell module for pathways: IFNγ signaling (D), TNF-α signaling (E), Oxidative
766 Phosphorylation (F), and Th2 signature (G) across disease conditions, shown on UMAP
767 embeddings. (H) Violin plots of gene expression for key MC markers (*CMA1*, *TPSG1*,
768 *LOC699599*) across disease conditions. (I) Cell counts of different MC subtypes (MC_C, MC_T,
769 MC_{TC}) across disease conditions (PTB, red bars, LTBI, blue bars, and HC green bars). (J)
770 UMAP plot of the NHP lung granuloma dataset (GSE200151), showing the distribution of cells

771 at 4 weeks (high disease burden) and 10 weeks (low disease burden) in *M. fasicularis* infected
772 with *Mtb Erdman*. (K) Gene expression violin plots for key MC markers (*CMA1*, *TPSG1*,
773 *LOC699599*) from the new dataset across time points. (L) Proportions of different MC subtypes
774 (MC_C, MC_T, MC_{TC}). (M) Violin plots of summed module scores for the key pathways (IFNγ
775 signaling, TNF-α signaling, oxidative phosphorylation) across disease burdens, showing
776 pathway activity. Statistical significance was assessed using Kruskal-Wallis tests with Dunn's
777 multiple comparison correction (**$p < 0.01$, ***$p < 0.001$, ****$p < 0.0001$).
778
779 **Figure 3: MC-deficient mice are resistant to *Mtb* chronic infection.**
780 (A) C57BL/6 and $CgKitW^{sh}$ mice were infected with a low aerosol dose (~100CFU) of *Mtb*
781 HN878 and mice were sacrificed at 50, 100 and 150 dpi. (B) Bacterial burden was assessed in
782 lungs and spleens by plating. (C) Lungs were harvested, fixed in formalin and embedded in
783 paraffin. H&E staining was carried out for blinded and unbiased analysis of histopathology.
784 (D) Representative images and the area of inflammation measured in each lobe are shown.
785 Scale bars: 2mm. Original magnification: ×20. Data points represent the mean ± SD of two
786 experiments (n = 8-15 per time point per group). Statistical analysis was performed using
787 unpaired, 2-tailed Student's t test between C57BL/6 and *CgKitW*^{sh} mice, **** $p < 0.0001$, ***
788 $p < 0.001$, * $p < 0.05$.
789
790 **Figure 4: MC-deficient mice have dysregulated immune profile after *Mtb* infection.**
791 C57BL/6 and *CgKitW*^{sh} mice were infected with a low aerosol dose (~100CFU) of *Mtb* HN878
792 and mice were sacrificed at 50, 100 and 150 dpi. Number of (A) MCs, (B) DCs (C) RMs, (D)
793 neutrophils (E)AMs, and (F) monocytes were enumerated in the lungs of *Mtb*-infected mice.
794 (G) Cytokine and chemokine production in lung homogenates from mice, collected at 150 dpi,
795 was assessed by multiplex cytokine analysis. Data points represent the mean ± SD of 1 of 2

796 individual experiments (n = 4-10 per time point per group). Statistical analysis was performed
797 using unpaired, 2-tailed Student's t test for (A) to (F) and Two-way ANOVA Sidak's multiple
798 comparison test for (G) between C57BL/6 and *CgKitW*^{sh} mice, *** $p < 0.0001$, ** $p < 0.001$,
799 * $p < 0.05$. Outliers were removed from the subsets using Grubb's outlier test.

800 **Figure 5: Wild-type mice with airway transferred MCs promote bacterial dissemination.**
801 Bone marrow derived in vitro cultured MCs ($5x10^4$ cells/mouse) were adoptively transferred
802 into the lung airways of C57BL/6 mice 7 days before infecting with a low aerosol dose
803 (~100CFU) of *Mtb* HN878. MCs were replenished in these mice at 15 dpi, and mice were
804 sacrificed at 30 dpi. Frequencies of (A) MCs, (B) neutrophils, and (C) RMs were enumerated
805 in the lungs of *Mtb*-infected mice. Bacterial burden was assessed in (D) lungs and (E)spleens
806 by plating. (F) Lungs were harvested, fixed in formalin, and embedded in paraffin. H&E
807 staining was carried out for blinded and unbiased analysis of histopathology. (G)
808 Immunofluorescence microscopy shows more neutrophil infiltration in the lungs of MC-
809 transferred WT mice. (H) $Ly6G^+$ cells per area of lung granuloma measured in each lobe are
810 shown. Scale bars: 2mm. Original magnification: ×20. Data points represent the mean ± SD.
811 Statistical analysis was performed using an unpaired, 2-tailed Student's t test between the
812 groups, **** $p < 0.0001$, *** $p < 0.001$, * $p < 0.05$.

813

814 **Figure S1: Predominance of MC_Ts in human and NHPs lung interstitium, blood vessels**
815 **and bronchi.** Healthy lung tissue and TB infected biopsies from human and NHP samples
816 were stained for MC_T (green), MC_C (red). Accumulation and localization of (A) MC_{TS}, (B)
817 MC_{CS}, and (C) MC_{TCS} in healthy and TB infected human lung, and (D) MC_{TS} and (E) MC_{TCS}
818 in LTBI and TB macaque lungs. Statistical analysis was performed using unpaired, 2-tailed
819 Student's t test, *** $p < 0.0001$, ** $p < 0.001$, * $p < 0.05$.

820 **Figure S2: Immune cell marker expression and pathway analysis across disease**
821 **conditions.** Data was re-analyzed from the lungs of NHPs (GSE200151). (A) UMAP
822 embeddings of MCs showing expression of cell surface markers: *FCER1A*, *MS4A2*, *CD48*, and
823 *ITGAX* across identified clusters. (B) Dot plot showing the expression levels of select genes
824 across clusters, where the dot size represents the percentage of cells expressing each gene, and
825 the color intensity represents the average expression level. (C) Violin plot of summed module
826 scores for IFNγ signaling, Oxidative Phosphorylation (D), TNF-α signaling (E), Th2 signature
827 (F) pathway across different disease conditions: LTBI/HC (green), PTB (pink), and the
828 respective clusters. (G) UMAP embeddings show the expression of key MC markers, including
829 *TPSG1*, *LOC699599*, and *CMA1* across identified clusters, with color intensity indicating
830 expression levels. Statistical significance was assessed using Kruskal-Wallis tests with Dunn's
831 multiple comparison correction (**$p < 0.01$, ***$p < 0.001$, ****$p < 0.0001$, ns: not significant).
832
833 **Figure S3: MCs appear at early *Mtb* infection.** C57BL/6 mice were infected with a low
834 aerosol dose (~100CFU) of *Mtb* HN878 and mice were sacrificed at 5, 21and 30 dpi. (A) The
835 number of MCs in the lungs was enumerated in *Mtb*-infected mice. (B) Bacterial burden was
836 assessed by plating. Data points represent the mean ± SD (n = 4-5 per time point). Statistical
837 analysis was performed using an unpaired, 2-tailed Student's t test between time points, *** p
838 < 0.0001, ** $p < 0.001$, * $p< 0.05$.
839 **Figure S4: MC-deficient mice have no baseline differences in T cell numbers.**
840 Six weeks C57BL/6 mice and *CgKitW*^{sh} mice were sacrificed to enumerate baseline numbers
841 of (A) $CD4^+$ T cells, and (B) $CD8^+$ T cells. Data points represent the mean ± SD (n = 4-5 per
842 time point).
843

844 **Figure S5: MC-deficient mice have reduced numbers of activated $CD4^+$ and $CD8^+$ T cells**
845 **in the lung.** C57BL/6 and $CgKitW^{sh}$ mice were infected with a low aerosol dose (~100CFU)
846 of *Mtb* HN878 and mice were sacrificed at 50, 100 and 150 dpi. Number of (A) $CD4^+$ $CD44^+$T
847 cells, (B) $CD4^+$ $CD44^+$ $IFN\gamma^+$ T cells, (C) $CD4^+$ $CD44^+$TNF-α^+ T cells (D) $CD4^+$ $CD44^+$ $IFN\gamma^+$
848 TNF-α^+ T cells, (E) $CD8^+$ $CD44^+$T cells, (F) $CD8^+$ $CD44^+$ $IFN\gamma^+$ T cells, (G) $CD8^+$ $CD44^+$
849 TNF-α^+ T cells, and (H) $CD8^+$ $CD44^+$ $IFN\gamma^+$ TNF-α^+ T cells in the lungs of *Mtb* infected mice.
850 Data points represent the mean ± SD of 1 of 2 individual experiments (*n* = 4-10 per time point
851 per group). Statistical analysis was performed using unpaired, 2-tailed Student's t test between
852 C57BL/6 and $CgKitW^{sh}$ mice, *** $p < 0.0001$, ** $p < 0.001$, * $p< 0.05$. Outliers were removed
853 from the subsets using Grubb's outlier test.
854 **Figure S6: Lung myeloid cell accumulation did not vary in MC-transferred WT *Mtb*-**
855 **infected mice.**
856 Bone marrow derived in vitro cultured MCs (n=50,000 cells per mouse) were adoptively
857 transferred into the lung airways of WT mice 7 days before infecting with a low aerosol dose
858 (~100CFU) of *Mtb* HN878. MCs were replenished in these mice at 15 dpi, and mice were
859 sacrificed at 30 dpi. Numbers of (A) MCs, (B) neutrophils, and (C) RMs were enumerated in
860 the lungs of *Mtb*-infected mice. Data points represent the mean ± SD of 1 of 2 individual
861 experiments (*n* = 4 per group).
862

863

864

865

866

867

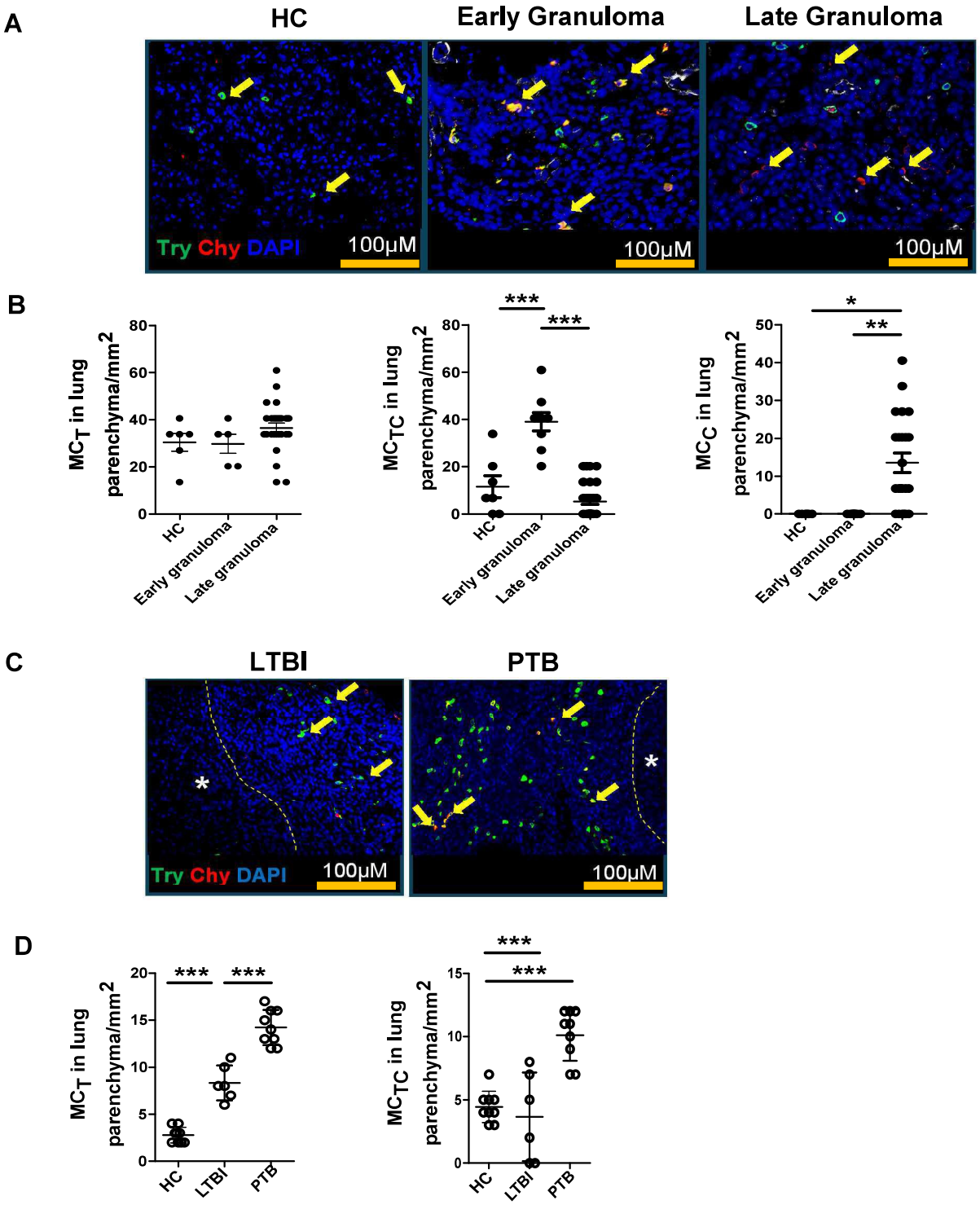
A
HC
Early Granuloma
Late Granuloma
Try Chy DAPI
100μM
B
MCT in lung parenchyma/mm2
MCTC in lung parenchyma/mm2
MCC in lung parenchyma/mm2
HC
Early granuloma
Late granuloma
***
*
**
C
LTBI
PTB
D
HC
LTBI
PTB

Figure 1

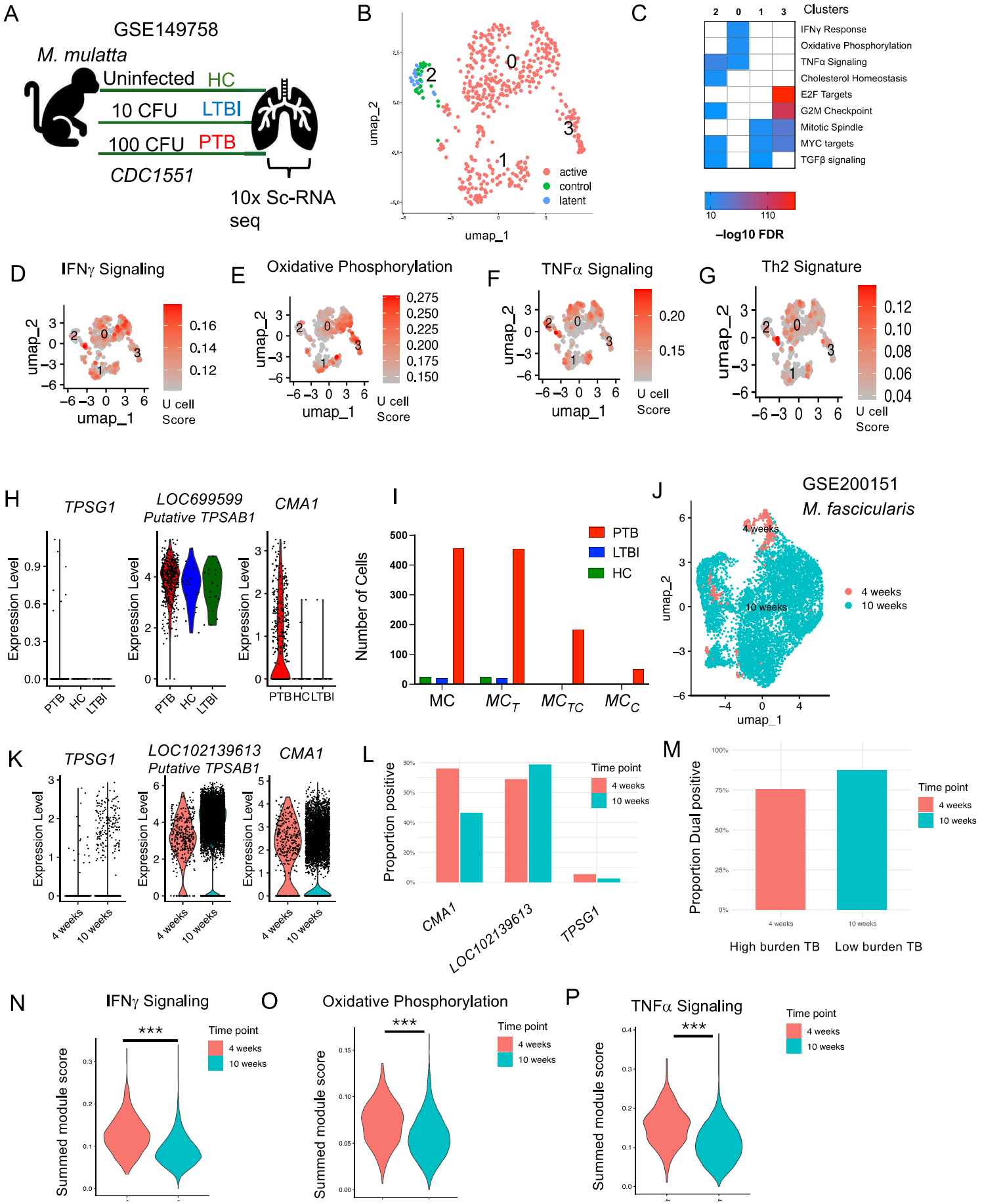
A
GSE149758
M. mulatta
Uninfected HC
10 CFU LTBI
100 CFU PTB
CDC1551
10x Sc-RNA seq
B
umap_2
umap_1
active
control
latent
C
Clusters
IFNγ Response
Oxidative Phosphorylation
TNFα Signaling
Cholesterol Homeostasis
E2F Targets
G2M Checkpoint
Mitotic Spindle
MYC targets
TGFβ signaling
–log10 FDR
D IFNγ Signaling
E Oxidative Phosphorylation
F TNFα Signaling
G Th2 Signature
U cell Score
H
TPSG1
LOC699599
Putative TPSAB1
CMA1
Expression Level
PTB
HC
LTBI
I
Number of Cells
MC
MC_T
MC_TC
MC_C
J
GSE200151
M. fascicularis
4 weeks
10 weeks
umap_2
umap_1
K
LOC102139613
L
Proportion positive
Time point
M
Proportion Dual positive
High burden TB
Low burden TB
N IFNγ Signaling
O Oxidative Phosphorylation
P TNFα Signaling
Summed module score
***

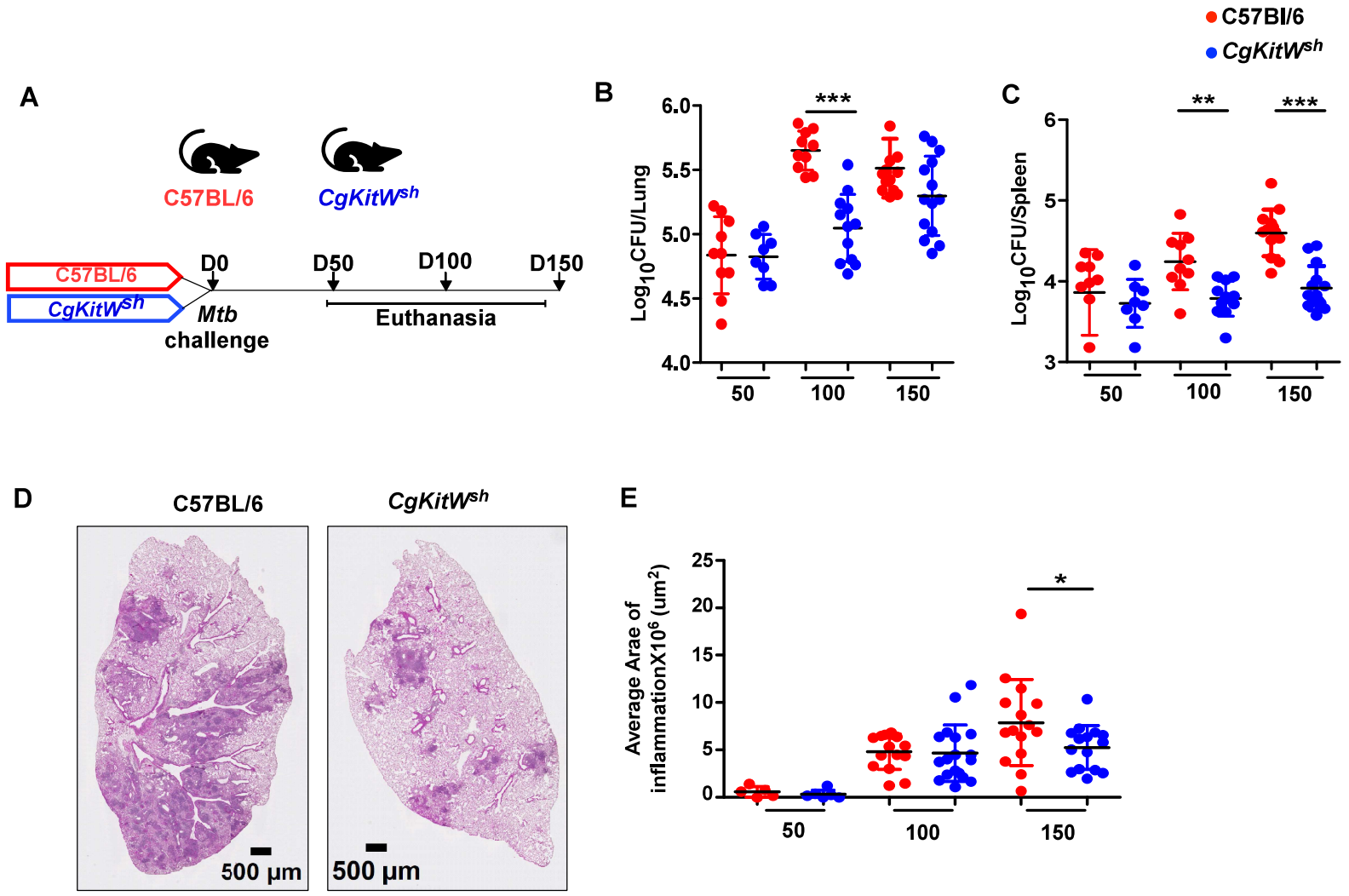
C57Bl/6
CgKitWsh
A
C57BL/6
CgKitWsh
C57BL/6
CgKitWsh
D0
D50
D100
D150
Mtb
challenge
Euthanasia
B
Log10CFU/Lung
6.0
5.5
5.0
4.5
4.0
***
50
100
150
C
Log10CFU/Spleen
6
5
4
3
**
***
50
100
150
D
C57BL/6
CgKitWsh
500 µm
500 µm
E
Average Arae of
inflammationX10^6 (um^2)
25
20
15
10
5
0
*
50
100
150

Figure 3

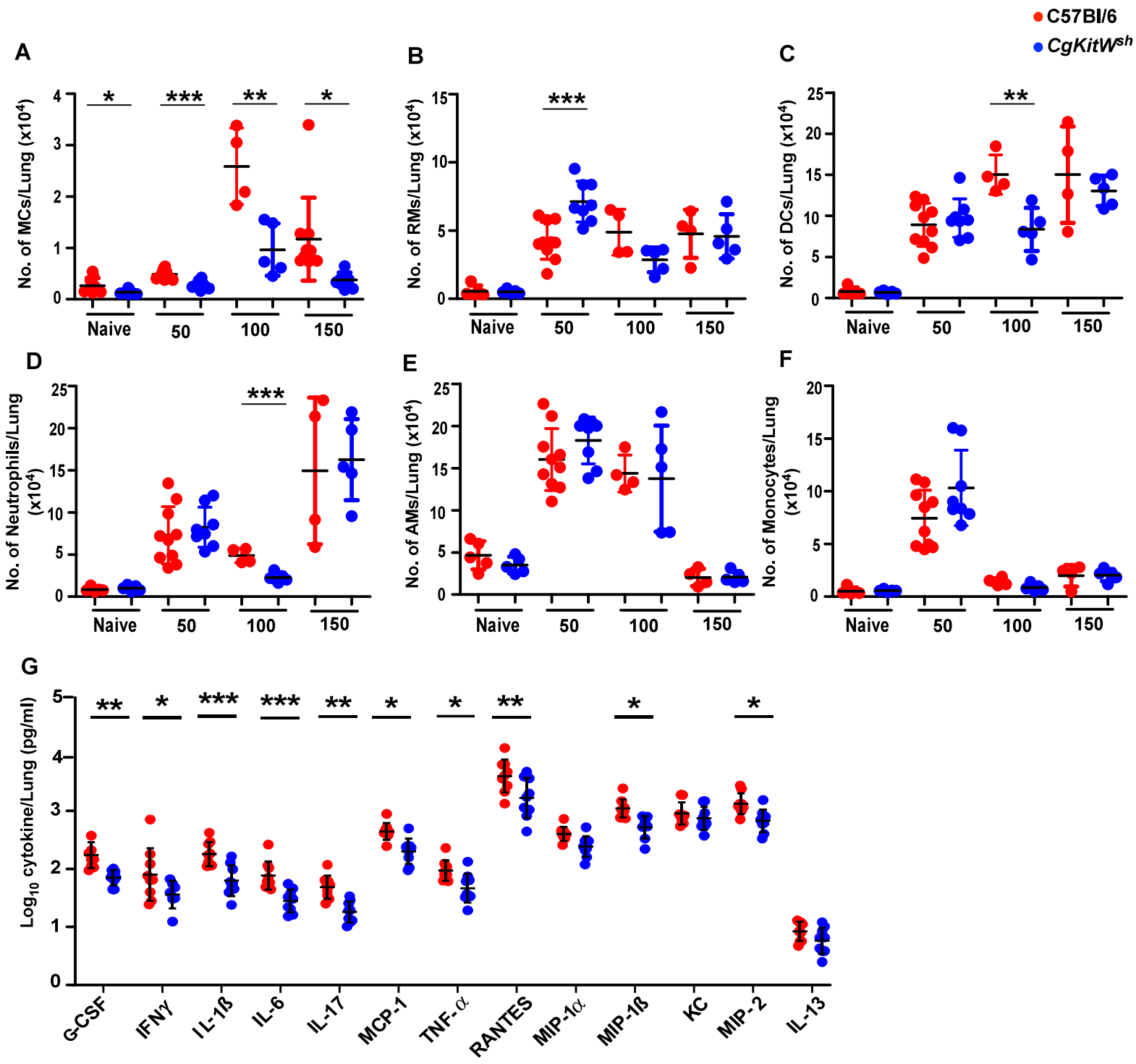
C57Bl/6
CgKitW^sh
A
No. of MCs/Lung (x10^4)
Naive
50
100
150
B
No. of RMs/Lung (x10^4)
C
No. of DCs/Lung (x10^4)
D
No. of Neutrophils/Lung (x10^4)
E
No. of AMs/Lung (x10^4)
F
No. of Monocytes/Lung (x10^4)
G
Log10 cytokine/Lung (pg/ml)
G-CSF
IFNγ
IL-1ß
IL-6
IL-17
MCP-1
TNF-α
RANTES
MIP-1α
MIP-1ß
KC
MIP-2
IL-13

Figure 4

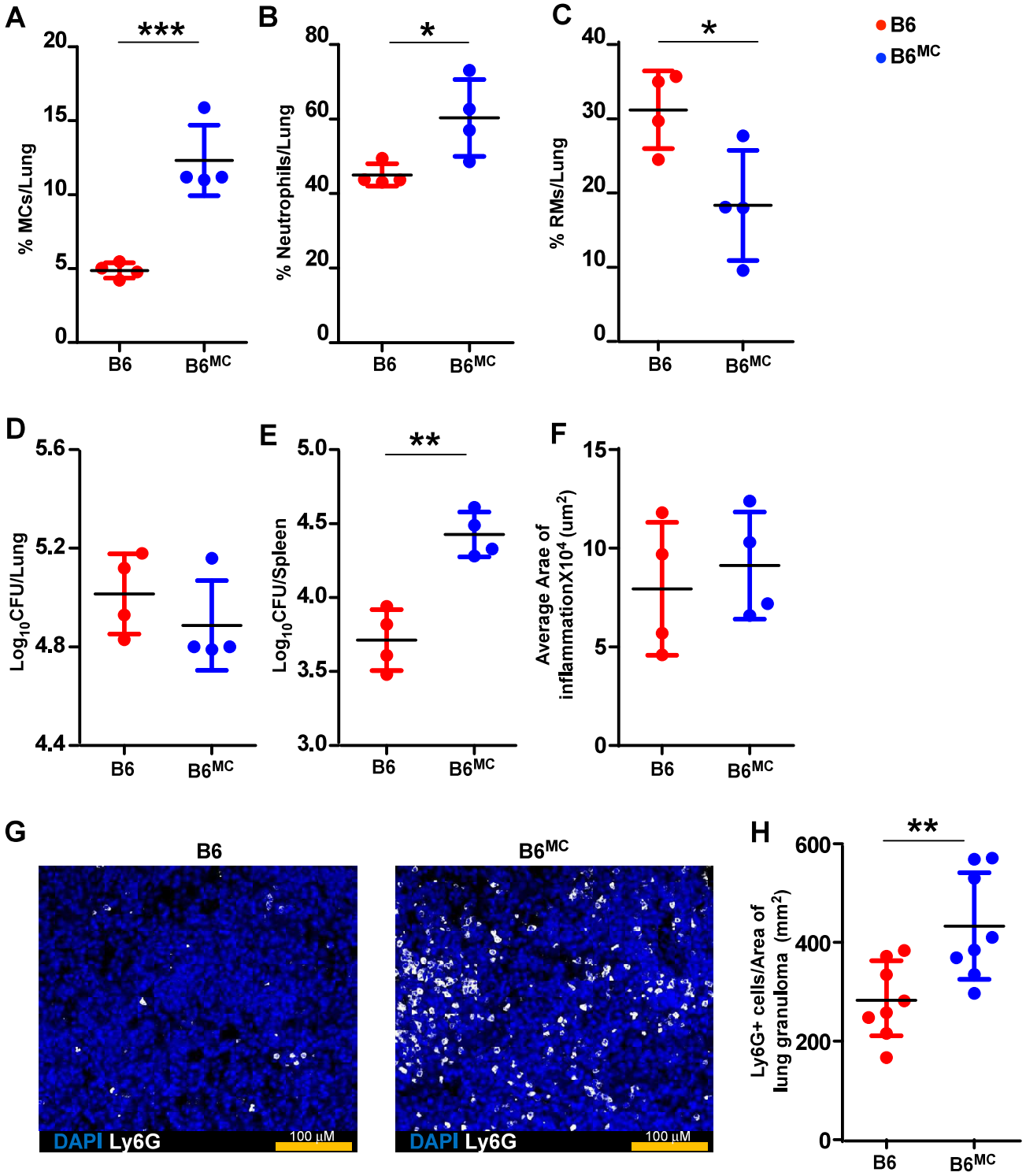
A
***
% MCs/Lung
20
15
10
5
0
B6
B6MC
B
*
% Neutrophils/Lung
80
60
40
20
0
B6
B6MC
C
*
% RMs/Lung
40
30
20
10
0
B6
B6MC
B6
B6MC
D
Log10CFU/Lung
5.6
5.2
4.8
4.4
B6
B6MC
E
**
Log10CFU/Spleen
5.0
4.5
4.0
3.5
3.0
B6
B6MC
F
Average Arae of inflammationX10^4 (um^2)
15
10
5
0
B6
B6MC
G
B6
B6MC
DAPI Ly6G
100 µM
DAPI Ly6G
100 µM
H
**
Ly6G+ cells/Area of lung granuloma (mm^2)
600
400
200
0
B6
B6MC

Figure 5

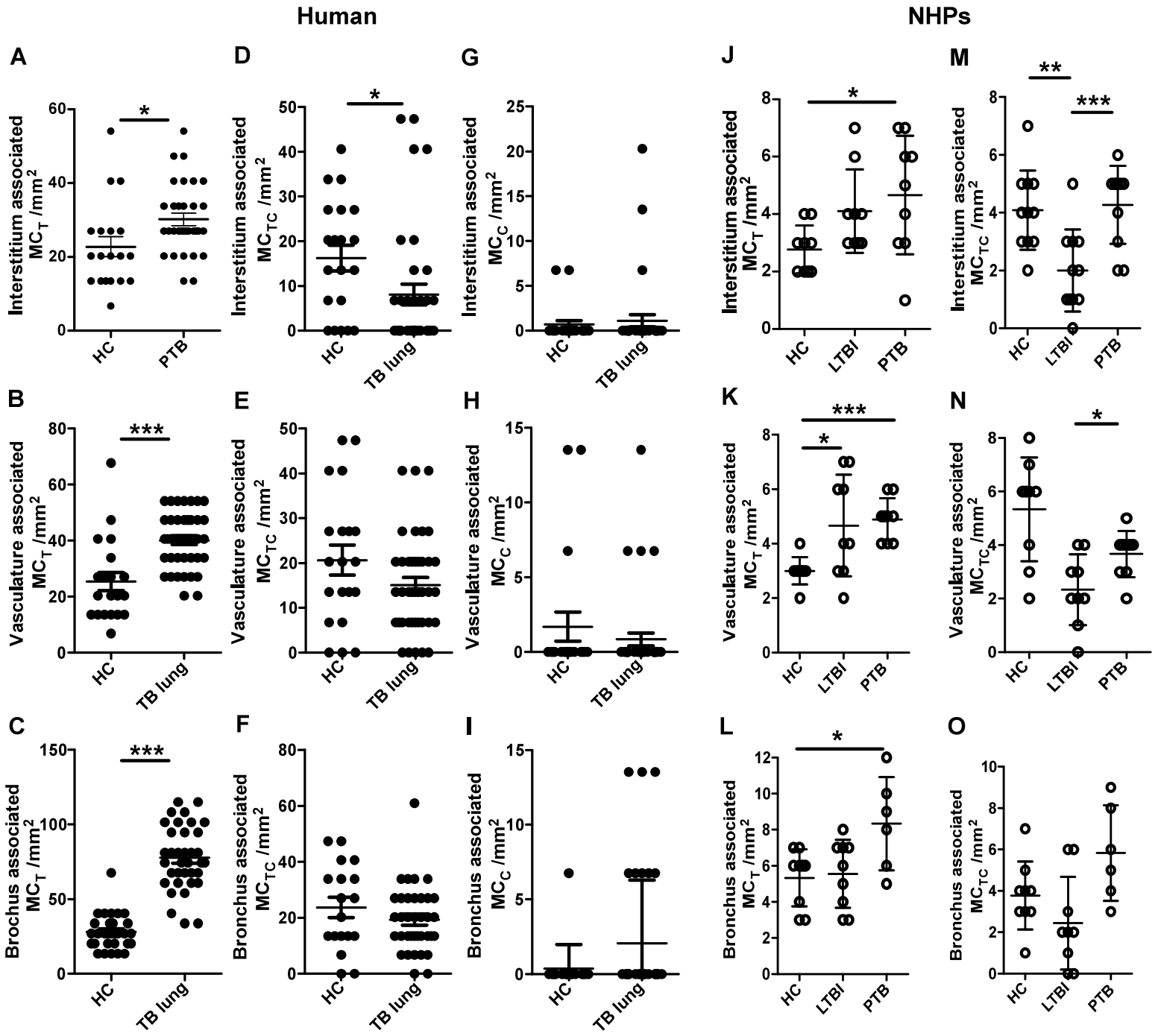
Human
NHPs
A
B
C
D
E
F
G
H
I
J
K
L
M
N
O
Interstitium associated MC_T /mm2
Vasculature associated MC_T /mm2
Brochus associated MC_T /mm2
Interstitium associated MC_TC /mm2
Vasculature associated MC_TC /mm2
Bronchus associated MC_TC /mm2
Interstitium associated MC_C /mm2
Vasculature associated MC_C /mm2
Bronchus associated MC_C /mm2
HC
PTB
TB lung
LTBI
*
**
***

Figure S1

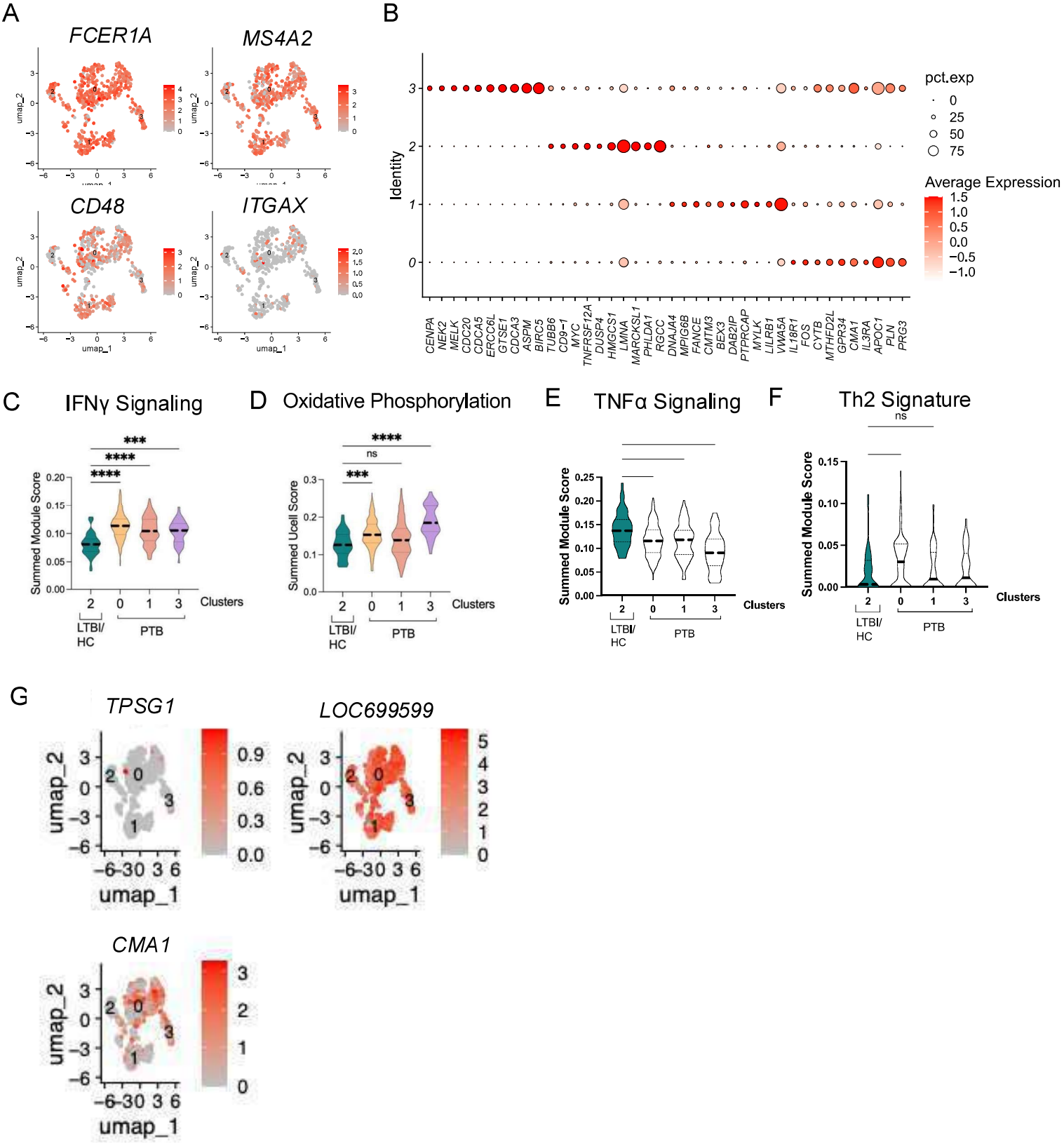
A
FCER1A
MS4A2
CD48
ITGAX
umap_1
umap_2
B
Identity
pct.exp
0
25
50
75
Average Expression
1.5
1.0
0.5
0.0
−0.5
−1.0
CENPA
NEK2
MELK
CDC20
CDCA5
ERCC6L
GTSE1
CDCA3
ASPM
BIRC5
TUBB6
CD9−1
MYC
TNFRSF12A
DUSP4
HMGCS1
LMNA
MARCKSL1
PHLDA1
RGCC
DNAJA4
MPIG6B
FANCE
CMTM3
BEX3
DAB2IP
PTPRCAP
MYLK
LILRB1
VWA5A
IL18R1
FOS
CYTB
MTHFD2L
GPR34
CMA1
IL3RA
APOC1
PLN
PRG3
C
IFNγ Signaling
Summed Module Score
Clusters
LTBI/
HC
PTB
D
Oxidative Phosphorylation
Summed Ucell Score
ns
E
TNFα Signaling
F
Th2 Signature
G
TPSG1
LOC699599
CMA1

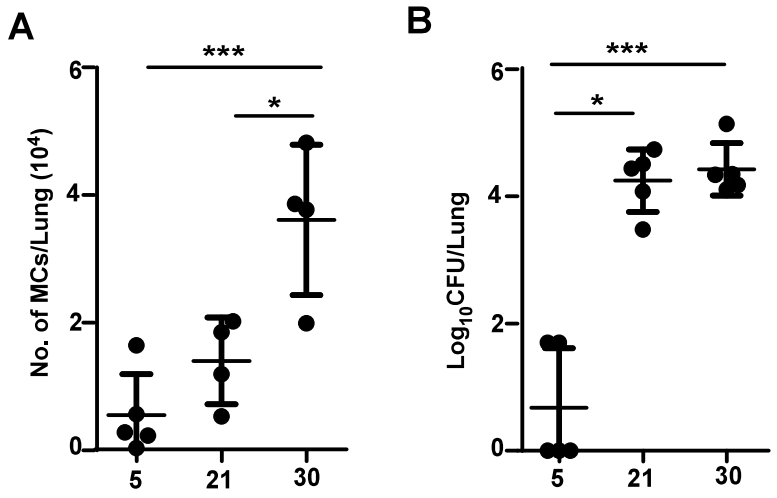

Figure S3

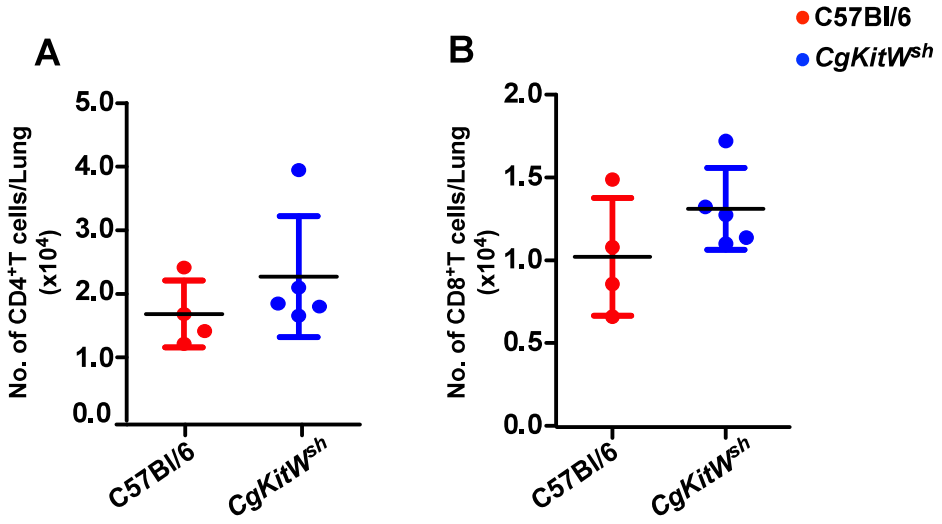
A
B
C57Bl/6
CgKitWsh
No. of CD4+T cells/Lung (x10^4)
5.0
4.0
3.0
2.0
1.0
0.0
No. of CD8+T cells/Lung (x10^4)
2.0
1.5
1.0
0.5
0.0
C57Bl/6
CgKitWsh

Figure S4

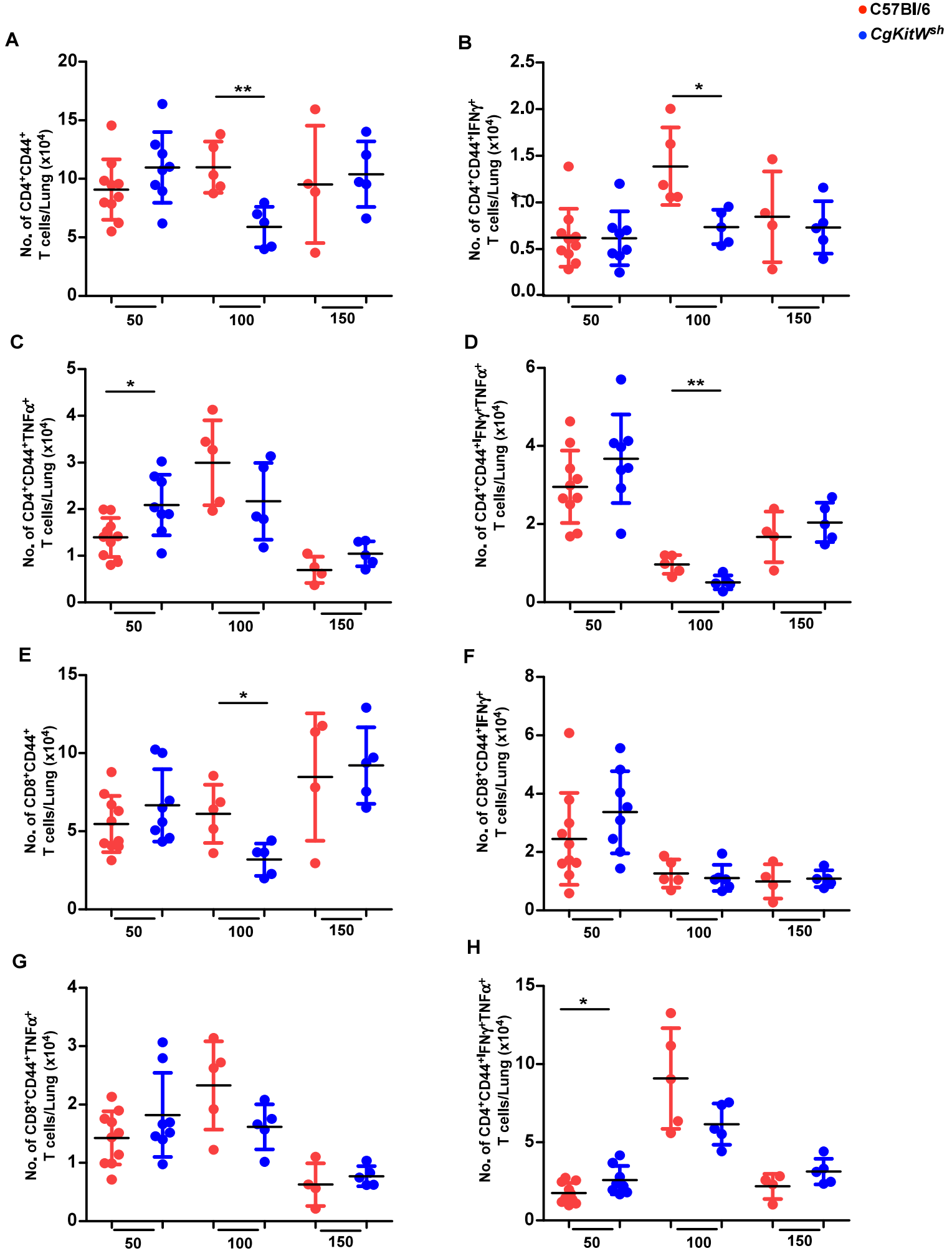
C57Bl/6
CgKitW^sh
A
No. of CD4+CD44+ T cells/Lung (x10^4)
**
B
No. of CD4+CD44+IFNγ+ T cells/Lung (x10^4)
*
C
No. of CD4+CD44+TNFα+ T cells/Lung (x10^4)
*
D
No. of CD4+CD44+IFNγ+TNFα+ T cells/Lung (x10^4)
**
E
No. of CD8+CD44+ T cells/Lung (x10^4)
*
F
No. of CD8+CD44+IFNγ+ T cells/Lung (x10^4)
G
No. of CD8+CD44+TNFα+ T cells/Lung (x10^4)
H
No. of CD4+CD44+IFNγ+TNFα+ T cells/Lung (x10^4)
*
50
100
150

Figure S5

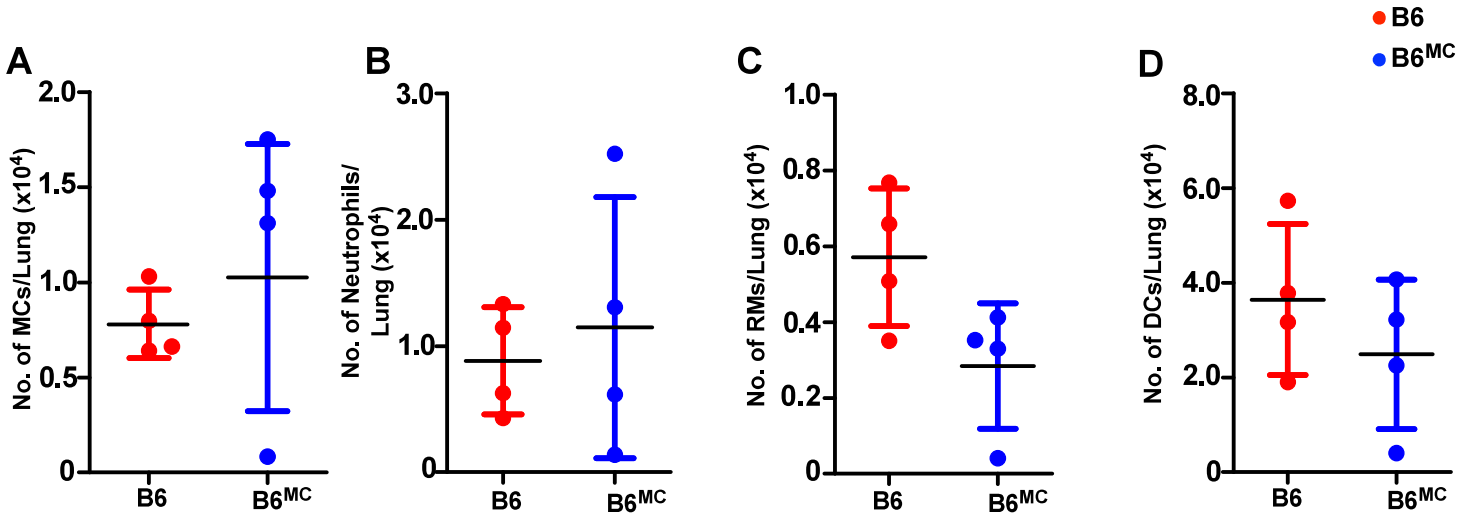
B6
B6MC
A
No. of MCs/Lung (x10^4)
2.0
1.5
1.0
0.5
0
B6
B6MC
B
No. of Neutrophils/ Lung (x10^4)
3.0
2.0
1.0
0
B6
B6MC
C
No. of RMs/Lung (x10^4)
1.0
0.8
0.6
0.4
0.2
0
B6
B6MC
D
No. of DCs/Lung (x10^4)
8.0
6.0
4.0
2.0
0
B6
B6MC

Figure S6